PERGAMON

International Journal of Solids and Structures 37 (2000) 3841–3871

INTERNATIONAL JOURNAL OF SOLIDS and STRUCTURES

www.elsevier.com/locate/ijsolstr

# A study of the coarsening in tin/lead solders

W. Dreyer[a], W.H. Müller[b,*]

[a]*Weierstraß Institut für Angewandte Analysis und Stochastik Mohrenstraße 39, 10117 Berlin, Germany*
[b]*Department of Mechanical and Chemical Engineering, Heriot-Watt University, Riccarton, Edinburgh, EH14 4AS, UK*

Received 15 October 1998; in revised form 29 April 1999

**Abstract**

This paper presents a model, which is capable to simulate the coarsening process observed during thermo-mechanical treatment of binary tin–lead solders. Fourier transforms and spectral theory are used for the numerical treatment of the thermo-elastic as well as of the diffusion problem encountered during phase separation in these alloys. More specifically, the analysis is based exclusively on continuum theory and, first, relies on the numerical computation of the local stresses and strains in a representative volume element. Second, this information is used in an extended diffusion equation to predict the local concentrations of the constituents of the solder. Besides the classical driving forces for phase separation, as introduced by Fick and Cahn–Hilliard, this equation contains an additional term which links the mechanical to the thermodynamical problem. It connects internal and external stresses, strains, temperature, as well as concentrations and allows for a comprehensive study of the coarsening and aging process. 

*Keywords:* Solder; Coarsening; Phase field models; Phase separation

## 1. Introduction

Joining methods are critical for the reliable use of electronic packages. In particular, since the advent of surface mount technology (SMT) the reliability and lifetime of solder joints has been one of the paramount topics in the field of modern microelectronic packaging technology (Lau and Rice, 1985). The first two pictures in Fig. 1 show a cross-sectional cut through the solder joint[1] of a micro-resistor, before and after thermal cycling between $-55^{\circ}C$ and $+125^{\circ}C$ according to military specification Mil-Std-883, method 1011. The third picture presents a cross-sectional cut through a solder ball of another

* Corresponding author. Tel.: +44-0131-451-3689; fax: +44-0131-451-3129.
*E-mail address:* w.h.muller@hw.ac.uk (W.H. Müller).

[1] All joints shown are made of eutectic tin–lead solder.

0020-7683/00/$ - see front matter 
PII: S0020-7683(99)00146-8

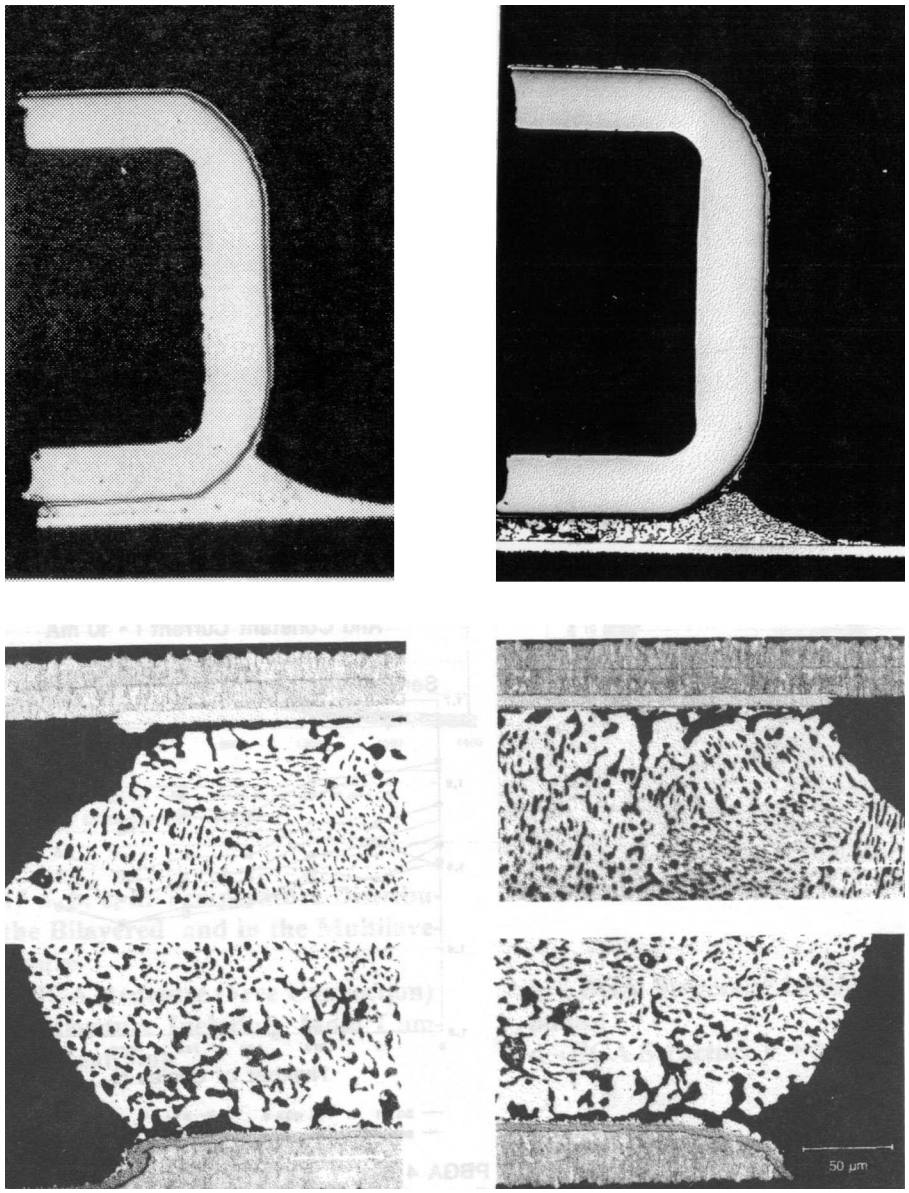


Fig. 1. Aging of Sn–Pb solder joints used in SMT (Jendrny et al., 1997; Albrecht and Gamalski, 1996).

microelectronic application, a ball grid array (BGA), after several thousand so-called power cycles. In this particular case, the microelectronic chip in the BGA serves as a heat source and leads to accelerated aging of the solder as follows.

The regions of different shades of grey and black in the various solder joints indicate that the originally fine mix between tin (Sn) and lead (Pb) is superseded by 'island formation' of high lead and tin concentrations. These form as a result of the separation of both phases, an aging process which is

known as 'coarsening' (Ozmat, 1990, p. 959; Harris et al., 1991, p. 20; Pao, 1992, p. 559). More specifically, coarsening in SnPb solders must be attributed to the combined effect of three mechanisms.

The first mechanism is classical diffusion which initiates the process of coarsening and which can be described mathematically by Fick's law (see, e.g., Rothman, 1984, p. 3). This process is particularly active at temperatures beyond 0.5°C of the homologous temperature of the solder which explains the effectiveness of accelerated aging tests, such as the aforementioned power-cycling. In fact, finite element studies have shown (Hauck et al., 1996) that power cycling can lead to local temperatures in the solder balls which are in the order of 150°C and more which corresponds to homologous temperatures greater than 0.9°C.[2]

The second mechanism is surface tension which controls the number, steepness, orientation, and the final shape of the interfaces within the coarsened structure. Mathematically speaking, this effect can be assessed by an additional term in the diffusional flux which was originally suggested by Cahn and Hilliard (1958). For the outcome of the final microstructure it is important to note that the size of the surface tensions varies by several order of magnitudes depending on whether the interfaces are coherent, semicoherent, or incoherent (Raghavan and Cohen, 1975, p. 77 ). Moreover, the size of the surface tensions is also influenced by temperature and, as it was emphasized before by Cahn and Hilliard (1958), p. 259, it can vary in the different directions of the crystal lattice. The latter will explain the typical eutectic structure observed in SnPb solders.

Third, thermo-mechanical stresses will also lead and enforce coarsening of a Sn–Pb microstructure (Seyyedi et al., 1991, p. 51; Hacke et al., 1997, p. 781; Nylén et al., 1997, p. 890). Their contribution to the diffusional flux is based on eigenstrains, which, locally, are due to the different thermal expansion lattice parameters of the anisotropic phases, and, globally, to the mismatch of the various materials involved in a microelectronics structure.

Consequently, as a result of the coarsening process, the overall material properties of the solder must change over time. This will eventually have a detrimental effect on the mechanical stability of the joint. For example, the creep behavior of a solder is directly linked to grain size (Darveaux et al., 1995, p. 397; Hacke et al., 1997), and the process of phase separation will lead to a decrease of the flow stress (Seyyedi et al., 1991, p. 51). The micro-morphology of the solder will also influence the crack path during the fracture process (Logsdon et al., 1990, p. 205). Moreover, for near-eutectic SnPb solder bumps, which are attached to an interposer through several pads made of copper and/or nickel, localized coarsening is accompanied by the formation of intermetallics in the highly stressed interfacial areas which precedes cracking (see the interface regions in the micrographs of Fig. 1, Hwang and Lucey, 1993, p. 663; Flanders et al., 1997).

From a technological point of view it is important to identify the factors that result in coarsening in solders. Once they are known and quantified it can be determined how to minimize their influence in order to increase the lifetime and the reliability of a solder joint and, hence, the electronic component. Eventually, it may also become possible to change these properties by suitable doping agents or external stress conditions such that healing of the solder material is initiated. However, in order to identify the factors quantitatively a realistic model, based on continuum theory, needs to be developed first. The development of this model and first *qualitative* simulations of the coarsening phenomenon with realistic material data for SnPb solders are the prime objectives of this paper.

However, in a second step, experiments must be carried out which allow the measurement of material parameters to be used during *quantitative* numerical simulations. The development of such an

[2] The homologous temperature is defined as the ratio between the current temperature and the melting temperature of the alloy, i.e., 183°C in the case of a eutectic Sn–Pb solder.

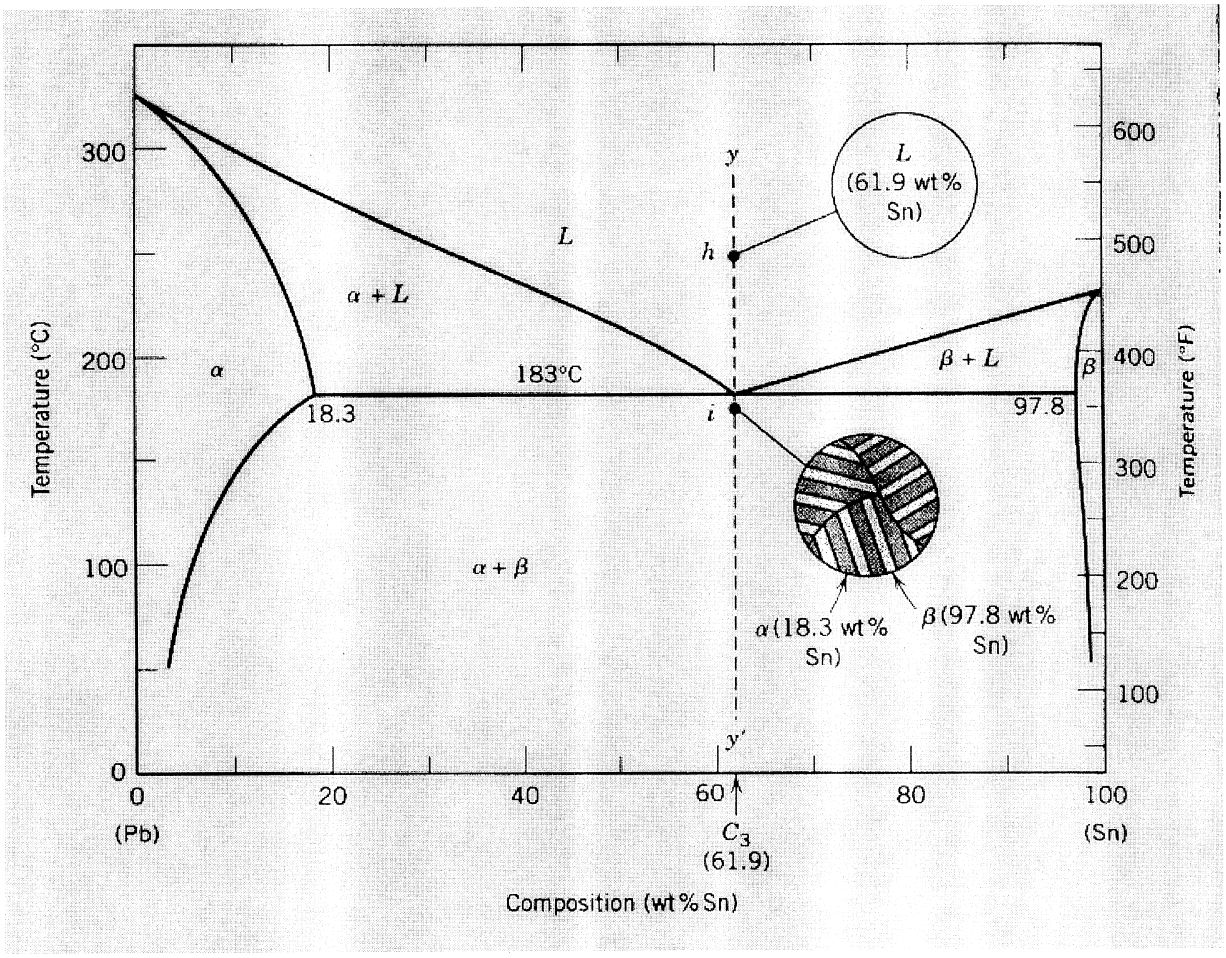


Fig. 2. The phase diagram of the binary alloy SnPb according to Callister (1997).

analytically *and* experimentally correlated simulation tool for the quantitative description of coarsening in a binary alloy is the long-term goal of the authors.

## 2. The mathematical model

### 2.1. Assumptions and objectives

Consider a body, $B$, which consists of a binary alloy of Pb and Sn at a eutectic composition[3] (see the phase diagram shown in Fig. 2). This body is divided into Representative Volume Elements (RVEs) which are characterized by material coordinates $\underline{x} = (x_1, x_2, x_3)$ in space. In order to avoid additional

[3] For simplicity this paper concentrates on the eutectic composition and the model will be geared toward the modeling of the eutectic microstructure.

complications the size of the RVE is such that it lies within one grain and grain boundaries need not to be modeled. Within the RVE there are regions of two different phases, the $\alpha$-phase which is rich in lead, and the $\beta$-phase which is rich in tin (cf., Fig. 2). The $\alpha$-phase has cubic material symmetry and the $\beta$-phase has tetragonal symmetry (i.e., the symmetry of their dominant elements, lead and tin, respectively).

From the mathematical point of view, the final objective of the model is to determine the strain fields, $\varepsilon_{ij}(\underline{x},t)$, and the field of the concentration of the tin, $c(\underline{x},t) = c_{\mathrm{Sn}}(\underline{x},t)$, for all points, $\underline{x} \in B$, and at all times, $t$. With the exception of the Appendix A we will assume in this paper that the temperature distribution, $T(t)$, within the body $B$ is homogeneous and a known ('given') function of time. Moreover, for a binary mixture only one concentration field needs to be determined since, due to mass conservation, the following identity holds:

$$c_{\mathrm{Sn}}(\underline{x},t) + c_{\mathrm{Pb}}(\underline{x},t) = 1. \tag{2.1}$$

### 2.2. The mechanical aspects of the model

It will be assumed that mechanical equilibrium is much faster to achieve than thermodynamical (or chemical) equilibrium. Consequently, the mechanical part of the problem or, in other words, the solution for the strain fields is based on the equation for static equilibrium of forces, i.e.,

$$\frac{\partial \sigma_{ij}}{\partial x_j} = 0, \tag{2.2}$$

where the symbol $\sigma_{ij}$ denotes the stress tensor. In addition to these equations, kinematic conditions and Hooke's law will be taken into account:

$$\varepsilon_{kl} = \frac{1}{2}\left(\frac{\partial u_k}{\partial x_l} + \frac{\partial u_l}{\partial x_k}\right), \quad \sigma_{ij} = C_{ijkl}\left(\varepsilon_{kl} - \varepsilon^*_{kl}\right), \tag{2.3}$$

where $\varepsilon_{kl}$ denotes the local total strains, $\varepsilon^*_{kl}$ are the 'eigenstrains' (i.e., nonelastic strains, such as thermal expansion, phase transformation, etc.; see Mura, 1987), and $C_{ijkl}$ is the stiffness matrix. Initially, when the SnPb-crystal develops from the melt, the eigenstrains originate as a consequence of the coherency of the different crystal lattices of the two phases. However, the simulation and study of the nucleation phase is left to future research. In this work we concentrate on the case of an already existing incoherent structure which will inevitably result since the lattice constants of the cubic $\alpha$-phase and tetragonal $\beta$-phase of SnPb solder are extremely different. Then the eigenstrains result from different thermal expansion of the two phases and, therefore, we put:

$$\varepsilon^*_{kl}(\underline{x},t) = \alpha_{kl}(\underline{x},t) \cdot (T - T_R), \quad \alpha_{kl}(\underline{x},t) = \theta(\underline{x},t)\alpha^{\alpha}_{kl} + \big(1 - \theta(\underline{x},t)\big)\alpha^{\beta}_{kl}, \tag{2.4}$$

where $T_R$ is the reference temperature of the stress-free state which, in the present case, was chosen to be the solidus temperature of the eutectic solder. The symbols $\alpha^{\alpha}_{ij}$ and $\alpha^{\beta}_{ij}$ are tensors of thermal expansion coefficients of the cubic $\alpha$-phase and tetragonal $\beta$-phase, respectively:

$$\alpha^{\alpha}_{ij} = \begin{pmatrix} \alpha^{\alpha} & 0 & 0 \\ 0 & \alpha^{\alpha} & 0 \\ 0 & 0 & \alpha^{\alpha} \end{pmatrix}, \quad \alpha^{\beta}_{ij} = \begin{pmatrix} \alpha^{\beta}_1 & 0 & 0 \\ 0 & \alpha^{\beta}_1 & 0 \\ 0 & 0 & \alpha^{\beta}_3 \end{pmatrix}. \tag{2.5}$$

To a first-order approximation the elements of these matrices are given by the thermal expansion coefficients of *pure* lead and tin. In order to account for higher order terms Vegard's law (see Massalski, 1965) or rules of mixtures could be used to relate them to the thermal expansion coefficients of the pure materials. However, in view of the uncertainty of the other material parameters involved in the model this will not be done in this paper.

The shape function, $\theta(\underline{x},t)$, of Eq. (2.4) is defined by:

$$\theta(\underline{x},t) = \frac{c^{\beta} - c(\underline{x},t)}{c^{\beta} - c^{\alpha}} \Longrightarrow \theta(\underline{x},t) = \begin{cases} 0 & \text{if } \underline{x} \in \beta \\ 1 & \text{if } \underline{x} \in \alpha \end{cases}, \tag{2.6}$$

where $c^{\beta}$ and $c^{\alpha}$ are the equilibrium concentrations of the $\alpha$- and $\beta$-phase. For a given temperature the equilibrium concentrations are constants, and they can be read off from the phase diagram shown in Fig. 2. Therefore, the eigenstrains are directly connected to the local (continuous) composition, $c(\underline{x},t)$, of the alloy. The shape function is also used to characterize the spatial dependence of other material parameters, such as the local stiffness:

$$C_{ijkl}(\underline{x},t) = \theta(\underline{x},t) C^{\alpha}_{ijkl} + \big(1 - \theta(\underline{x},t)\big) C^{\beta}_{ijkl}, \tag{2.7}$$

the tensor of surface tensions:

$$a_{ij}(\underline{x},t) = \theta(\underline{x},t) a^{\alpha}_{ij} + \big(1 - \theta(\underline{x},t)\big) a^{\beta}_{ij}, \tag{2.8}$$

and the matrix of mobility coefficients:

$$M(\underline{x},t) = \theta(\underline{x},t) M^{\alpha} + \big(1 - \theta(\underline{x},t)\big) M^{\beta}. \tag{2.9}$$

The indices $\alpha$ and $\beta$ in these equations refer to properties of the $\alpha$- and $\beta$-phase, respectively, which are assumed to be constant and known material quantities. Specifically, for the stiffness tensor, Voigt's coefficients, $C^{\alpha/\beta}_{ij}$, are preferably used in data handbooks. They are related to $C^{\alpha/\beta}_{ijkl}$ as follows:

| $\frac{kl}{ij}$ | 11 | 22 | 33 | 23 | 31 | 12 |
|---|---|---|---|---|---|---|
| 11 | $C^{\alpha}_{11}$ | $C^{\alpha}_{12}$ | $C^{\alpha}_{12}$ | 0 | 0 | 0 |
| 22 | $C^{\alpha}_{12}$ | $C^{\alpha}_{11}$ | $C^{\alpha}_{12}$ | 0 | 0 | 0 |
| 33 | $C^{\alpha}_{12}$ | $C^{\alpha}_{12}$ | $C^{\alpha}_{11}$ | 0 | 0 | 0 |
| 23 | 0 | 0 | 0 | $C^{\alpha}_{44}$ | 0 | 0 |
| 31 | 0 | 0 | 0 | 0 | $C^{\alpha}_{44}$ | 0 |
| 12 | 0 | 0 | 0 | 0 | 0 | $C^{\alpha}_{44}$ |

,

| $\frac{kl}{ij}$ | 11 | 22 | 33 | 23 | 31 | 12 |
|---|---|---|---|---|---|---|
| 11 | $C^{\beta}_{11}$ | $C^{\beta}_{12}$ | $C^{\beta}_{13}$ | 0 | 0 | 0 |
| 22 | $C^{\beta}_{12}$ | $C^{\beta}_{11}$ | $C^{\beta}_{13}$ | 0 | 0 | 0 |
| 33 | $C^{\beta}_{13}$ | $C^{\beta}_{13}$ | $C^{\beta}_{33}$ | 0 | 0 | 0 |
| 23 | 0 | 0 | 0 | $C^{\beta}_{44}$ | 0 | 0 |
| 31 | 0 | 0 | 0 | 0 | $C^{\beta}_{44}$ | 0 |
| 12 | 0 | 0 | 0 | 0 | 0 | $C^{\beta}_{66}$ |

. (2.10)

Initially, a suitable function of position will be assumed for $c(\underline{x},t)$ (e.g., nuclei in form of localized tin-rich regions), which, by virtue of Eqs. (2.4)–(2.6), provides an initial condition for the eigenstrains $\varepsilon^{*}_{kl}$. The resulting stresses and strains will then be computed from Eqs. (2.2) and (2.3). In the next subsection it will be discussed how this can be achieved for the initial time as well as during the subsequent time steps.

### 2.3. Solution of the mechanical problem

Recently spectral methods or, more specifically, *discrete Fourier transforms* (DFT) have been used in an extremely promising way to solve stress/strain problems in heterogeneous solids (e.g., Canuto et al., 1988; Suquet, 1990; Moulinec and Suquet, 1994, 1998; Dreyer (1994); Dreyer et al., 1998; Müller, 1996, 1998a, 1998b; Müller and Neumann, 1998). Specifically we will consider the case that loads $\sigma^0_{xx}$, $\sigma^0_{xy}$, $\sigma^0_{yy}$ are specified along the periphery of the RVE (cf., Fig. 3, left) are specified as follows:

$$\int_{2\pi L} \sigma_{xx}\,\mathrm{d}y + \int_{2\pi L} \sigma_{xy}\,\mathrm{d}y = \left(\sigma^0_{xx} + \sigma^0_{xy}\right)2\pi L, \quad \int_{2\pi L} \sigma_{yy}\,\mathrm{d}x + \int_{2\pi L} \sigma_{xy}\,\mathrm{d}x = \left(\sigma^0_{yy} + \sigma^0_{xy}\right)2\pi L, \tag{2.11}$$

where $\sigma_{xy}$ follows from the solution of Eqs. (2.2) and (2.3). Following Müller (1998a) we consider an array of $N$ points, $\underline{x}$, in a physical space of dimension $d$, arranged equidistantly over a square unit cell lattice of length $L$ (see Fig. 3, right):

$$\underline{x} = h\underline{\alpha}, \qquad \underline{\alpha} = (\alpha_1, \ldots, \alpha_d), \quad \alpha_j \in \{0,1,\ldots,N-1\},\ (j,d) \in \{1,2,3\},\ h = \frac{2\pi L}{N}. \tag{2.12}$$

Let discrete field variables, $f(\underline{\alpha})$, be defined in each of these points. Then the *discrete Fourier transform* for these variables can be obtained by summation:

$$\hat{f}(\underline{s}) = \frac{1}{N^{d/2}} \sum_{\alpha_1=0}^{N-1} \cdots \sum_{\alpha_d=0}^{N-1} f(\underline{\alpha}) \exp\left(\mathrm{i}2\pi \frac{\underline{s}\cdot\underline{\alpha}}{N}\right) \equiv Y\left[f(\underline{\alpha})\right]. \tag{2.13}$$

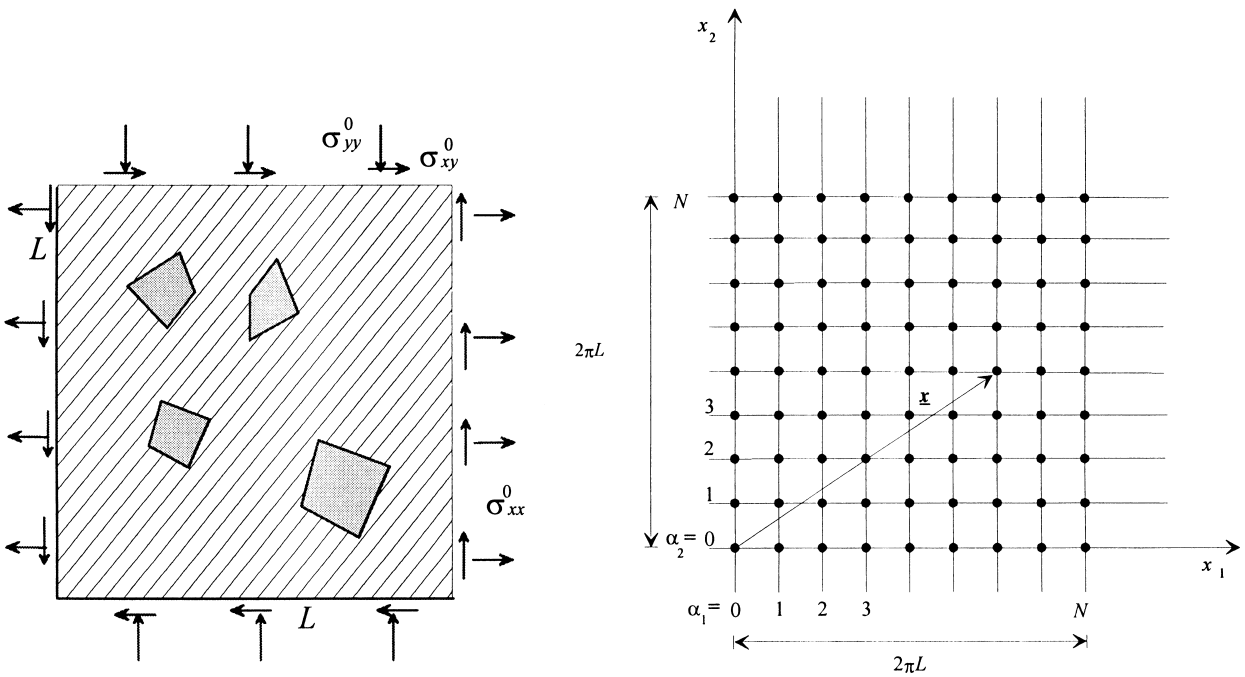


Fig. 3. Square RVE and its discretization in the two-dimensional case, $N = 8$.

If *periodicity conditions* hold across the representative volume element, RVE:

$$f(\underline{\alpha}+N\underline{r})=f(\underline{\alpha}),\quad \underline{r}=(r_1,\ldots,r_d),\ r_j\in Z \tag{2.14}$$

the corresponding quantities $f(\underline{\alpha})$ in physical space can be obtained through Fourier's theorem provided that $\hat{f}(\underline{s})$ is known:

$$f(\underline{\alpha})=\frac{1}{N^{d/2}}\sum_{s_1=0}^{N-1}\cdots\sum_{s_d=0}^{N-1}\hat{f}(\underline{s})\exp\left(-\mathrm{i}\frac{2\pi}{N}\underline{s}\cdot\underline{\alpha}\right). \tag{2.15}$$

Note that all summations are *finite* and can be performed exactly, e.g., by fast Fourier transform. The sums do *not* represent an approximation of continuous Fourier integrals. As in the continuous case, a differentiation rule holds:

$$Y\left(\frac{\partial f(\underline{\alpha})}{\partial x_j}\right)=\xi_j(s_j)Y\big(f(\underline{\alpha})\big)+O(h^2),\quad \xi_j(s_j)=-\frac{i}{h}\sin\left(\frac{h}{L}s_j\right). \tag{2.16}$$

This rule is an approximation of spatial differentiation by a central difference quotient and it is based on the *shift theorem* which requires the *periodicity conditions* (2.14) to hold. Second derivatives can be treated similarly:[4]

$$Y\left(\frac{\partial^2 f(\underline{\alpha})}{\partial x_j^2}\right)=\xi_{\underline{jj}}(s_j)Y\big(f(\underline{\alpha})\big)+O(h^2),\qquad \xi_{\underline{jj}}(s_j)=\frac{2}{h^2}\left(\cos\left(\frac{h}{L}s_j\right)-1\right),$$

$$Y\left(\frac{\partial^2 f(\underline{\alpha})}{\partial x_i\partial x_j}\right)=\xi_{ij}(s_i,s_j)Y\big(f(\underline{\alpha})\big)+O(h^2),\qquad \xi_{ij}(s_i,s_j)=-\frac{1}{h^2}\sin\left(\frac{h}{L}s_i\right)\sin\left(\frac{h}{L}s_j\right),\quad i\neq j. \tag{2.17}$$

DFT will now be applied to Eqs. (2.2) and (2.3), i.e., to static, linear-elastic problems with small deformations and to solve the resulting PDE of second order. To this end we make use of the equivalent inclusion technique (EIT) which goes back to Eshelby (Mura, 1987). This method circumvents the problem of the spatial dependence of the stiffness matrix by introducing an auxiliary strain field $\varepsilon^H_{kl}(\underline{\alpha})$ (Moulinec and Suquet, 1998; Müller, 1998a) and an auxiliary *constant* stiffness matrix, $C^H_{ijkl}$, as follows:

$$\sigma_{ij}(\underline{\alpha},t)=C_{ijkl}(\underline{\alpha},t)\big(\varepsilon_{kl}(\underline{\alpha},t)-\varepsilon^*_{kl}(\underline{\alpha},t)\big)=C^H_{ijkl}\big(\varepsilon_{kl}(\underline{\alpha},t)-\varepsilon^*_{kl}(\underline{\alpha},t)-\varepsilon^H_{kl}(\underline{\alpha},t)\big). \tag{2.18}$$

If this is inserted into Eqs. (2.2) and (2.3) the following problem remains to be solved:

$$C^H_{ijkl}\frac{\partial^2}{\partial x_j\partial x_l}u_k=C^H_{ijkl}\frac{\partial}{\partial x_j}\big(\varepsilon^H_{kl}+\varepsilon^*_{kl}\big). \tag{2.19}$$

Periodicity of all fields is assumed and by virtue of the differentiation theorems (2.16) and (2.17) this system of PDEs is mapped onto a system of linear equations in Fourier space for which one formal solution can be obtained as follows:

$$\varepsilon_{kl}(\underline{\alpha},t)=Y^{-1}\Big[\hat{A}^H_{klop}\hat{\varepsilon}^H_{op}\Big](\underline{\alpha},t)+Y^{-1}\Big[\hat{A}^H_{klop}\hat{\varepsilon}^*_{op}\Big](\underline{\alpha},t)+\varepsilon^0_{kl}, \tag{2.20}$$

[4] Some of the indices are underlined in order to indicate that no summation is implied.

where compare Falk (1966) for the case of asimilar "singularity" at $s = \underline{0}$:

$$\hat{A}^{H}_{ijkl} = \begin{cases} 0, & \underline{s} = \underline{0} \\ \dfrac{1}{2D}\left(\xi_i N_{js} + \xi_j N_{is}\right) C^{H}_{srkl}\xi_r, & \underline{s} \neq \underline{0}. \end{cases} \tag{2.21}$$

The symbols $N_{js}$ and $D$ are the discriminant and determinant of the following matrix:

$$M_{ik} = C^{H}_{ijkl}\xi_{jl} \Longrightarrow M^{-1}_{ik} = \frac{N_{ik}}{D}. \tag{2.22}$$

They are cumbersome but known functions of the stiffness $C^{H}_{ijkl}$ (which will soon be chosen suitably), and of the Fourier transforms of the difference quotients (2.17) which, for an arbitrary degree of anisotropy, are preferably determined by means of analytical software packages, such as Mathematica®. In particular, for the cubic phase, the following concise relations can be used directly:

$$D = -\mu\left(\lambda + 2\mu + \mu'\right)(\xi_{kk})^2 - \left(\lambda + \mu + \mu'\right)^2 \xi_{11}\xi_{22} + (\lambda + \mu)^2 \xi^2_{12},$$

$$N_{ij} = -\Big[\left(\lambda + 2\mu + \mu'\right)\xi_{kk}\delta_{ij} - (\lambda + \mu)\xi_{ij} - \mu'\delta_{ijkl}\xi_{kl}\Big], \tag{2.23}$$

where $\delta_{ij}$,$\delta_{ijkl}$ denote Kronecker symbols and $\lambda$, $\mu$ and $\mu'$ are Lamé's constants, respectively.

The choice $\hat{A}^{H}_{ijkl}(\underline{s} = \underline{0}) = 0$ implies that we currently consider the case of mean strains, $\varepsilon^0_{kl}$. In fact, mean strains are defined by:

$$\bar{\varepsilon}_{ij} = \frac{1}{N^d}\sum_{\alpha_1=0}^{N-1} \cdots \sum_{\alpha_d=0}^{N-1} \varepsilon_{ij}(\underline{\alpha}). \tag{2.24}$$

On the other hand, the definition of Fourier transforms according to Eq. (2.13) leads to:

$$\hat{\varepsilon}_{ij}(\underline{0}) = \frac{1}{(N)^{d/2}}\sum_{s_1=0}^{N-1} \cdots \sum_{s_d=0}^{N-1} \varepsilon_{ij}(\underline{\alpha}). \tag{2.25}$$

Mutual insertion of Eqs. (2.24) and (2.25) yields:

$$\bar{\varepsilon}_{ij} = \frac{1}{(N)^{d/2}}\hat{\varepsilon}_{ij}(\underline{0}), \tag{2.26}$$

and since (cf. Eqs. (2.20) and (2.21)):

$$\hat{\varepsilon}_{ij}(\underline{0}) = \hat{A}^{H}_{ijkl}(\underline{0})\hat{\varepsilon}^{H}_{kl}(\underline{0}) + \hat{A}^{H}_{ijkl}(\underline{0})\hat{\varepsilon}^{*}_{kl}(\underline{0}) + \varepsilon^0_{ij} = 0 \cdot \hat{\varepsilon}^{H}_{kl}(\underline{0}) + 0 \cdot \hat{\varepsilon}^{*}_{kl}(\underline{0}) + \varepsilon^0_{ij} = \varepsilon^0_{ij}, \tag{2.27}$$

it finally follows that:

$$\bar{\varepsilon}_{ij} = \varepsilon^0_{ij}. \tag{2.28}$$

The solution shown in Eqs. (2.20) and (2.21) solves the original PDE and, as well shall see shortly, it also enables us to take the boundary condition (2.11) into account. Next, we eliminate the auxiliary field $\hat{\varepsilon}^{H}_{op}$. To this end we insert Eqs. (2.7) and (2.20) into (2.18) to obtain:

$$C^{H}_{ijkl}\Big(Y^{-1}\Big[\hat{A}^{H}_{klop}\hat{\varepsilon}^{H}_{op}\Big](\underline{\alpha},t)+Y^{-1}\Big[\hat{A}^{H}_{klop}\hat{\varepsilon}^{*}_{op}\Big](\underline{\alpha},t)+\varepsilon^{0}_{kl}-\varepsilon^{*}_{kl}(\underline{\alpha},t)-\varepsilon^{H}_{kl}(\underline{\alpha},t)\Big)$$
$$=\Big(C^{\beta}_{ijkl}-\theta(\underline{\alpha},t)\Big[C^{\beta}_{ijkl}-C^{\alpha}_{ijkl}\Big]\Big)\Big(Y^{-1}\Big[\hat{A}^{H}_{klop}\hat{\varepsilon}^{H}_{op}\Big](\underline{\alpha},t)+Y^{-1}\Big[\hat{A}^{H}_{klop}\hat{\varepsilon}^{*}_{op}\Big](\underline{\alpha},t)+\varepsilon^{0}_{kl}-\varepsilon^{*}_{kl}(\underline{\alpha},t)\Big). \tag{2.29}$$

In what follows the 'growth' of the softer $\alpha$-phase in an initially uniform $\beta$-matrix will be studied. Then, in order to guarantee convergence, the constant matrix $C^{H}_{ijkl}$ should be chosen as (cf., Müller, 1998a):

$$C^{H}_{ikjl}=C^{\beta}_{ijkl}, \tag{2.30}$$

which results in:

$$C^{\beta}_{ijkl}\varepsilon^{H}_{kl}(\underline{\alpha},t)=\theta(\underline{\alpha},t)\Big(C^{\beta}_{ijkl}-C^{\alpha}_{ijkl}\Big)\Big(Y^{-1}\Big[\hat{A}^{\beta}_{klop}\hat{\varepsilon}^{H}_{op}\Big](\underline{\alpha},t)+Y^{-1}\Big[\hat{A}^{\beta}_{klop}\hat{\varepsilon}^{*}_{op}\Big](\underline{\alpha},t)+\varepsilon^{0}_{kl}-\varepsilon^{*}_{kl}(\underline{\alpha},t)\Big). \tag{2.31}$$

This is a functional equation for the unknown field $\varepsilon^{H}_{kl}(\underline{\alpha},t)$ which is solved in the standard Neumann fashion:

$$\overset{(n+1)}{\varepsilon}{}^{H}_{kl}(\underline{\alpha},t)=\theta(\underline{\alpha},t)\big(C^{\beta}\big)^{-1}_{klrs}\Big(C^{\beta}_{rsmn}-C^{\alpha}_{rsmn}\Big)\Bigg(Y^{-1}\Big[\hat{A}^{\beta}_{mnop}\overset{(n)}{\hat{\varepsilon}}{}^{H}_{op}\Big](\underline{\alpha},t)$$
$$+Y^{-1}\Big[\hat{A}^{\beta}_{mnop}\hat{\varepsilon}^{*}_{op}\Big](\underline{\alpha},t)+\varepsilon^{0}_{mn}-\varepsilon^{*}_{mn}(\underline{\alpha},t)\Bigg), \tag{2.32}$$

where the 0th iteration strain field, $\overset{(0)}{\varepsilon}{}^{H}_{ij}$, and $\varepsilon^{0}_{ij}$ are given by (i.e., the latter follows from the external loads imposed on a homogeneous RVE, cf., Fig. 3):

$$\overset{(0)}{\varepsilon}{}^{H}_{ij}=0,\quad \varepsilon^{0}_{ij}=(C^{-1})^{\beta}_{ijkl}\sigma^{0}_{kl}. \tag{2.33}$$

$Y^{-1}$ denotes the inverse discrete Fourier transform defined by Eqs. (2.13) and (2.14), and the symbols $\hat{A}^{\beta}_{mnop}$ can be computed from $\hat{A}^{H}_{mnop}$ (see Eq. (2.21)) if $C^{H}_{ijkl}$ is substituted by $C^{\beta}_{ijkl}$. In fact, EIT was originally developed for the continuum and Eq. (2.32) is the discrete counterpart of the Neumann iteration technique for the solution of a Fredholm integral equation for the continuous field $\varepsilon^{H}_{kl}(\underline{x})$. For completeness, it should be pointed out that in the present situation, for a given external net stress $\sigma^{0}_{ij}$, Eq. (2.33) for the strain field $\varepsilon^{0}_{ij}$ is also evaluated by using $C^{\beta}_{ijkl}$.

It should be noted that the relations for the thermal expansion coefficients, the stiffness tensor, the surface tensions, and for the mobility tensor shown in Eqs. (2.5) and (2.7)–(2.9) maintain their simple form only if the coordinate systems of the RVE, $x_i$, and of the crystallographic axes of the phases, $x'_j$, coincide. However, this will be the exception and in most cases both coordinate systems are linked to each other by a transformation matrix, $O^{\alpha/\beta}_{ij}$,[5] which is different from unity:

$$x_i=O^{\alpha/\beta}_{ij}x'_j. \tag{2.34}$$

Consequently,

$$\alpha^{\alpha/\beta}_{ij}=O^{\alpha/\beta}_{ir}O^{\alpha/\beta}_{js}\alpha'^{\,\alpha/\beta}_{rs} \tag{2.35}$$

[5] The suffix $\alpha/\beta$ indicates that both phases could still be oriented differently.

and

$$C^{\alpha/\beta}_{ijkl} = O^{\alpha/\beta}_{ir} O^{\alpha/\beta}_{js} O^{\alpha/\beta}_{kt} O^{\alpha/\beta}_{lu} C'^{\alpha/\beta}_{rstu}, \tag{2.36}$$

where the matrices $C'^{\alpha/\beta}_{rstu}$ and $\alpha'^{\alpha/\beta}_{rs}$ have the form as indicated before in Eqs. (2.10) and (2.5), respectively. Eqs. (2.35) and (2.36) can now be used to compute the local eigenstrains and stiffnesses according to Eqs. (2.4) and (2.7), as well as the symbols $\hat{A}^{\alpha/\beta}_{mnop}$ according to Eqs. (2.21) and (2.22). It should be pointed out that the symbolic computation of these symbols is extremely tedious, especially for tetragonal symmetry. In fact, this became only feasible by using various features of the Mathematica® software package to create a reliable FORTRAN file.

To summarize this subsection it seems worth recalling that loading of the body is taken into account in two ways: First, it can be due to internal eigenstrains, $\varepsilon^*_{kl}$. In the present case, these will evolve as a consequence of the different thermal expansion coefficients of the tin- and lead-rich phase.

Second, loading can also be imposed from outside by prescribing suitable mean averages for the stresses, $\sigma^0_{ij}$, along the boundary of the RVE: (see Eqs. (2.11) and (2.33)). Physically speaking, these are due to the global thermal mismatch of the microelectronic structure and/or to direct mechanical straining of the solder, e.g., by shear testing (see Nylén et al., 1997, p. 891).

### 2.4. The thermodynamical aspects of the model

Once the local stresses and strains are known at a certain time, $t$, they will be used to compute the evolvement of the distribution of concentrations, $c$, of during the next time-step, $\Delta t$. This follows from a numerical solution of the diffusion equation:

$$\rho_0 \frac{\partial c}{\partial t} + \frac{\partial J_i}{\partial x_i} = 0, \tag{2.37}$$

where $\rho_0$ is the total mass density with respect to the reference configuration, and $J_i$ is the following extended diffusion flux:

$$J_i = -\rho_0 M \frac{\partial}{\partial x_i}\left(\frac{\partial \psi}{\partial c} - a_{kl}\frac{\partial^2 c}{\partial x_k \partial x_l} + \frac{\partial}{\partial c}\left[\frac{1}{2}\left(\varepsilon_{kl} - \varepsilon^*_{kl}\right) C_{klrs}\left(\varepsilon_{rs} - \varepsilon^*_{rs}\right)\right]\right), \tag{2.38}$$

$M$ being the (scalar) mobility factor which will be related to the mobility of the $\alpha$- and $\beta$-phase as shown in Eq. (2.9).

Moreover, $\psi$ is the configurational part of the Gibbs' free energy density of the system, which will be assumed in form of a suitable Landau polynomial (see below). A sketch of the derivation of Eqs. (2.37) and (2.38) is presented in Appendix A.

Note that the first term in the diffusion flux leads to the classical diffusion equation as proposed by Fick (e.g., Rothman, 1984, p. 3), whereas the second part contains extensions of the diffusion equation as introduced by Cahn and Hilliard, $a_{ij}$ being a matrix of surface tension related quantities (see Cahn and Hilliard, 1958, and de Fontaine, 1975, or Hawick, 1991, Chapter 3, for a comprehensive summation of the original results which is related to the surface tension coefficients of the $\alpha$- and $\beta$-phase as shown in Eq. (2.8)).

Note that the diffusional flux shown in Eq. (2.38) contains an additional term which characterize the influence of mechanical stresses on the diffusion process *explicitly*:

$$\frac{\partial}{\partial c}\left(\frac{1}{2}\left(\varepsilon_{kl} - \varepsilon^*_{kl}\right) C_{klrs}\left(\varepsilon_{rs} - \varepsilon^*_{rs}\right)\right) = -\sigma_{kl}\frac{\partial \varepsilon^*_{kl}}{\partial c} + \frac{1}{2}\left(\varepsilon_{kl} - \varepsilon^*_{kl}\right)\frac{\partial C_{klrs}}{\partial c}\left(\varepsilon_{rs} - \varepsilon^*_{rs}\right). \tag{2.39}$$

As a result, the computed change in concentrations during the time $\Delta t$ will lead to a change of the micromorphology and, consequently, necessitates an update of the local stress/strain distribution in the RVE by means of Eqs. (2.32) and (2.33). If this has been achieved, the next time-step can be considered, etc. Some details of the numerical procedures involved will be presented in the next subsection.

In order to guarantee coexistence of both phases $\alpha$ and $\beta$ the density of the Gibbs' free energy needs to be a non-convex function of the concentrations, for example (see Cahn and Hilliard, 1958, p. 261; Tsakalakos, 1985, p. 150):

$$\psi = \psi_0\left(\left([c^\alpha - c_0]^2 - [c - c_0]^2\right)^2 - b[c - c_0]\right), \quad c_0 = \frac{1}{2}(c^\alpha + c^\beta), \tag{2.40}$$

where $\psi_0$ and $b$ are temperature dependent coefficients which need to be adjusted suitably (see Section (3.1)), and $c^\alpha$, $c^\beta$ are the equilibrium concentrations which were mentioned in Section (2.4).

### 2.5. Some remarks on the numerical treatment of the extended diffusion equation

The extended diffusion equations (2.37) and (2.38) are mapped into discrete Fourier space and the Fourier transforms of spatial differential quotients are replaced according to Eq. (2.17):

$$\frac{1}{M}\frac{\mathrm{d}\hat{c}}{\mathrm{d}t} = \xi_{ii}\left[Y\left(\frac{\partial\psi}{\partial c}\right) - Y\left(a_{kl}\frac{\partial^2 c}{\partial x_k \partial x_l}\right) + Y\left(\frac{\partial}{\partial c}\left[\frac{1}{2}(\varepsilon_{kl} - \varepsilon^*_{kl})C_{klrs}(\varepsilon_{rs} - \varepsilon^*_{rs})\right]\right)\right]. \tag{2.41}$$

To this end it was assumed that:

$$M^\alpha = M^\beta = M. \tag{2.42}$$

This was done mainly in view of the missing data regarding the mobility and diffusivity coefficients of both species. It is left to future research to make use of the additional possibilities Eq. (2.9) has to offer. A dimensionless time is introduced:

$$\tilde{t} = t\frac{M\psi_0}{L^2} = n\Delta\tilde{t}, \quad n \in N. \tag{2.43}$$

The time derivative is approximated in the usual manner, and an implicit scheme is used for its integration (cf., Küpper and Masbaum, 1994, p. 1850):

$$\begin{aligned}\frac{\hat{c}^{n+1} - \hat{c}^n}{\Delta\tilde{t}} = \tilde{\xi}_{ii}\Bigg[&Y\left(\frac{\partial\tilde{\psi}}{\partial c}\right)|_{\hat{c}=\hat{c}^n} - \tilde{a}^\beta_{kl}\tilde{\xi}_{kl}\hat{c}^{n+1} + \left(\tilde{a}^\beta_{kl} - \tilde{a}^\alpha_{kl}\right)Y\left(\theta\frac{\partial^2 c}{\partial\tilde{x}_k\partial\tilde{x}_l}\right)|_{\hat{c}=\hat{c}^n} - \\ &Y\left(\tilde{\sigma}_{kl}\frac{\partial\varepsilon^*_{kl}}{\partial c}\right)|_{\hat{c}=\hat{c}^n} + Y\left(\frac{1}{2}(\varepsilon_{kl} - \varepsilon^*_{kl})\frac{\partial\tilde{C}_{klrs}}{\partial c}(\varepsilon_{rs} - \varepsilon^*_{rs})\right)|_{\hat{c}=\hat{c}^n},\end{aligned} \tag{2.44}$$

with dimensionless quantities:

$$\tilde{\xi}_{jj}(s_j) = 2\left(\frac{N}{2\pi}\right)^2\left(\cos\left(\frac{2\pi}{N}s_j\right) - 1\right), \qquad \tilde{\xi}_{ij}(s_i, s_j) = -\left(\frac{N}{2\pi}\right)^2\sin\left(\frac{2\pi}{N}s_i\right)\sin\left(\frac{2\pi}{N}s_j\right), \quad i \neq j, \tag{2.45}$$

$$\tilde{\psi} = \frac{\psi}{\psi_0}, \quad \tilde{a}_{kl} = \frac{a_{kl}}{\psi_0 L^2}, \quad \tilde{\sigma}_{kl} = \frac{\sigma_{kl}}{\psi_0}, \quad \tilde{C}_{klrs} = \frac{C_{ijkl}}{\psi_0}, \quad \tilde{x}_l = \frac{x_l}{L}. \tag{2.46}$$

### 2.6. A brief comparison with the literature

DFT techniques have been used before solving extended diffusion equations, such as (2.37) and (2.38). Particularly noteworthy is the work of the school headed by Khachaturyan (see, e.g., Khachaturyan et al., 1995; Chen et al., 1991; McCormack et al., 1992; Wang et al., 1991, 1993a, 1993b, 1994; Wang and Khachaturyan, 1995, 1997), the papers of Nishimori and Onuki (1990); Li and Chen (1997) and Laberge et al. (1997), and the work by Koyama, Miyazaki and co-authors (e.g., Takeuchi et al., 1990; Miyazaki et al., 1991; Koyama et al., 1994, 1996; Koyama and Miyazaki, 1994, 1998; Mebed et al., 1997; Miyazaki and Koyama, 1996, 1997).

Even though there is a certain resemblance between the solution procedures used therein and the one outlined in Section (2.5), there are also fundamental differences, as follows:

- The physical concepts presented in the aforementioned papers are *not* based on the concepts of continuum theory alone. Rather they rely heavily on a microscopic formalism, also referred to as the stochastic field approach, which requires the use of kinetic coefficients together with atomic interaction energies, and fluctuation potentials.
- A complete continuum mechanics solution for the stress and strain fields, i.e., of Eqs. (2.2) and (2.3), is *not* performed. Rather the influence of the mechanical stresses and strains are taken into account indirectly. To this end the local elastic strain energy density is used (e.g., Li and Chen, 1997, Eq. (3); Koyama and Miyazaki, 1998, Eq. (22)) which is then evaluated by means of the Green's function solution shown in Eqs. (2.20) and (2.21). An average stiffness $C^{0}_{ijkl}$ is inserted there which, as it was pointed out by Li and Chen (1997), p. 1273, is an effective medium *approximation* which is legitimate provided the differences of the stiffnesses between the various phases are not too large. However, in the present case such an assumption seems questionable since the ratio of Young's moduli for (polycrystalline) tin and lead is roughly 3 : 1 (cf., Winter, 1998), and an iterative solution as shown in Eqs. (2.32) and (2.33) seems more appropriate.
- In the recent work by Koyama and Miyazaki (1998), Eq. (23), the local variation in stiffness is accounted for very similarly to Eq. (2.7). The only difference is the use of another shape function as the one shown in Eq. (2.6). If this difference is taken into account, and if one specializes to cubic symmetry the two mechanical contributions to the diffusion flux in Eqs. (2.38) and (2.39) are identical with their expression for the strain energy contribution to the chemical potential, $\mu_{\mathrm{str}}$, Eq. (26). However, the expression for the mobility as suggested by Koyama and Miyazaki (1998), Eq. (7), is clearly different from the one shown Eq. (2.9). For lack of data it is difficult to say how this difference influences the development of the microstructure. As it was mentioned before this aspect is left to future research.
- Simulations with materials that show a higher degree of anisotropy than cubic symmetry have not been reported by the aforementioned authors. As indicated before, some of their equations hold for cubic materials only. Also, no attempt was made to study the case where the axes of the RVE or, in other words, the orientation of the externally applied forces and the main crystallographic axes do not coincide.

## 3. Results and discussion

### 3.1. Choice of material constants

The thermal expansion coefficients and the elasticity constants of the lead- and tin-rich phase were approximated by the corresponding data for the pure elements (Lee and Raynor, 1955, p. 739; Handbook of Chemistry and Physics, 1995, pp. 12–38, 12–40, 12–172):

$$\alpha^{\alpha} = 28.9 \times 10^{-6}\ \mathrm{K}^{-1}, \quad \alpha_1^{\beta} = 16.7 \times 10^{-6}\ \mathrm{K}^{-1}, \quad \alpha_3^{\beta} = 36.4 \times 10^{-6}\ \mathrm{K}^{-1}, \tag{3.1}$$

$$C^{\alpha}_{11} = 49.66\ \mathrm{GPa}, \quad C^{\alpha}_{12} = 42.31\ \mathrm{GPa}, \quad C^{\alpha}_{44} = 14.98\ \mathrm{GPa}, \tag{3.2}$$

$$C^{\beta}_{11} = 75.29\ \mathrm{GPa}, \quad C^{\beta}_{12} = 61.56\ \mathrm{GPa}, \quad C^{\beta}_{13} = 44.00\ \mathrm{GPa},$$

$$C^{\beta}_{33} = 95.52\ \mathrm{GPa}, \quad C^{\beta}_{44} = 21.93\ \mathrm{GPa}, \quad C^{\beta}_{66} = 23.36\ \mathrm{GPa}. \tag{3.3}$$

The equilibrium concentrations of the $\alpha$- and $\beta$-phase, $c^{\alpha}$ and $c^{\beta}$, can be read off from the phase diagram shown in Fig. 2. Note that they are not symmetrically arranged in the following sense:

$$c^{\alpha} \neq 1 - c^{\beta}. \tag{3.4}$$

Indeed, if the temperature of the eutectic is increased from $-40^{\circ}\mathrm{C}$ to the melting temperature at $+183^{\circ}\mathrm{C}$, the concentration $c^{\alpha}$ shows a considerable variation between 1% and 18.3%, whereas $c^{\beta}$ changes by less than 3%. Two considerably different temperature levels have been selected:

$$T_{\mathrm{high}} = 150^{\circ}\mathrm{C}: \quad c^{\alpha} = 11.88\%,\ c^{\beta} = 97.98\%, \tag{3.5}$$

$$T_{\mathrm{low}} = 20^{\circ}\mathrm{C}: \quad c^{\alpha} = 1.54\%,\ c^{\beta} = 99.86\%. \tag{3.6}$$

Note that if the ordinary Maxwell or common tangent construction (Raynor, 1965, p. 293) is applied to the quadric chosen for the Gibbs' free energy in Eq. (2.37) the following result is obtained:

$$\frac{\partial \psi}{\partial c}|_{c=c^{\alpha}} = -\psi_0 b, \quad \frac{\partial \psi}{\partial c}|_{c=c^{\beta}} = -\psi_0 b, \quad \frac{\psi(c^{\beta}) - \psi(c^{\alpha})}{c^{\beta} - c^{\alpha}} = -\psi_0 b, \tag{3.7}$$

which is independent of the choice of $c^{\alpha}$ and $c^{\beta}$. In fact, the remaining factor, $b$, is irrelevant for the temporal evolution of the concentration profile (cf., Eqs. (2.37) and (2.38)) and, therefore, it is unnecessary to give it a value.

Reliable data for the various surface tension related quantities, $a^{\alpha}_{ij}$ and $a^{\beta}_{ij}$, of Eq. (2.8) is difficult to obtain. They will depend on the crystallographic direction just as the surface tensions in single crystals do (cf., Sundquist, 1964). To the best knowledge of the authors no data for the surface tensions of pure lead and tin single crystals is available. Nevertheless, the following statements can be made:

- Due to the dominance of the lead the $\alpha$-phase is cubic, and (cf., Cahn and Hilliard, 1958, p. 259) the matrix $a^{\alpha}_{ij}$ will be isotropic:

$$a^{\alpha}_{ij} = a^{\alpha}\delta_{ij}. \tag{3.8}$$

- Similarly, for the tetragonal $\beta$-phase, the matrix $a^{\beta}_{ij}$ must be diagonal with respect to the main crystallographic axes:

$$a^{\beta}_{ij} = \begin{pmatrix} a^{\beta}_1 & 0 & 0 \\ 0 & a^{\beta}_1 & 0 \\ 0 & 0 & a^{\beta}_3 \end{pmatrix}_{ij}. \tag{3.9}$$

- The crystal lattice parameters for pure lead and pure tin are given by (Winter, 1998):

$$r^{\mathrm{Pb}}_1 = r^{\mathrm{Pb}}_2 = r^{\mathrm{Pb}}_3 = 495.08\ \mathrm{pm}, \quad r^{\mathrm{Sn}}_1 = r^{\mathrm{Sn}}_2 = 583.18\ \mathrm{pm}, \quad r^{\mathrm{Sn}}_3 = 318.19\ \mathrm{pm}. \tag{3.10}$$

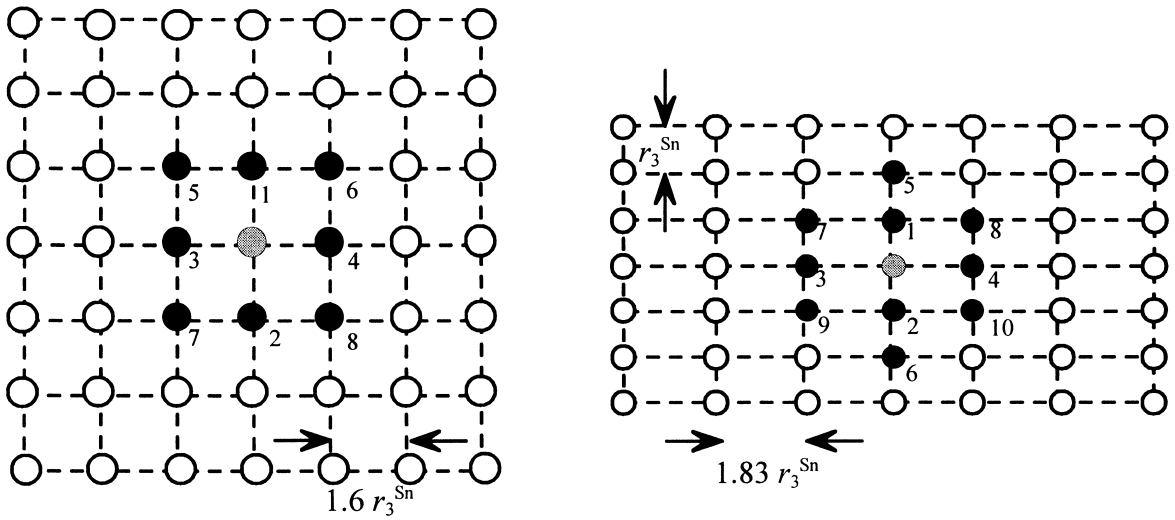


Fig. 4. Two-dimensional arrangement of a cubic lattice of Pb-atoms (left) and a tetragonal lattice of Sn-atoms (right), see text.

They depend on the temperature, and for a first-order approximation they can also be used to characterize the lattice parameters of the $\alpha$- and $\beta$-phase.[6] These parameters can now be used to rank the coefficients, $a^\alpha$, $a_1^\beta$, $a_1^\beta$, with respect to each other. For that purpose arguments similar to Cahn and Hilliard (1958), p. 262, are used to, first, arrive at the following formulae:

$$a^\alpha = \frac{1}{3}\sum_n Z_n r_n^2 \nu_n, \quad a_1^\beta = \frac{1}{2}\sum_n \left( Z_n - \sum_{\alpha=1}^{Z_n} \cos^2(\vartheta^\alpha) \right) r_n^2 \nu_n, \quad a_3^\beta = \sum_n \left( \sum_{\alpha=1}^{Z_n} \cos^2(\vartheta^\alpha) \right) r_n^2 \nu_n, \tag{3.11}$$

where $n$ identifies the coordination shell at a radius $r_n$ from a center point atom, $Z_n$ denotes the coordination number, $\vartheta^\alpha$ is the azimuthal angle which leads to atom $\alpha$, and:

$$\nu_n(r_n) = E_{AB}(r_n) - \frac{1}{2}\left[ E_{AA}(r_n) + E_{BB}(r_n) \right], \tag{3.12}$$

where $E_{AA}$, $E_{BB}$ and $E_{AB}$ are the inter-atomic potentials for the $n$th coordination shell which, for simplicity, are supposed to depend only on the radial distance, $r_n$. Second, again for simplicity, a two-dimensional arrangement of atoms is considered. This is shown in Fig. 4 where a representative atom (shaded in gray color) is surrounded by first- and second-order neighbors (in black). Typical distances relevant for lead and tin are also shown. The various sums of Eq. (3.11) are approximately evaluated up to second neighbors to yield:

$$a^\alpha \approx \frac{4}{3}\left(r_1^{Sn}\right)^2 \left[ \nu^{Pb}\left(r_1^{Sn}\right) + 2\nu^{Pb}\left(\sqrt{2} r_1^{Sn}\right) \right],$$

$$a_1^\beta \approx 10\left(r_1^{Sn}\right)^2 \nu^{Sn}\left(2r_1^{Sn}\right), \quad a_3^\beta = 2\left(r_1^{Pb}\right)^2 \left[ \nu^{Sn}\left(r_1^{Sn}\right) + 2\nu^{Sn}\left(2r_1^{Sn}\right) \right]. \tag{3.13}$$

[6] For these they change slightly according to Vegard's law (see Predel, 1991–1997, p. 185; Lee and Raynor, 1955).

Here an average value of $2r_1^{\mathrm{Sn}}$ has been used to assess atoms number 3 to 10 which are shown in Fig. 4. Following Cahn and Hilliard (1958), p. 263, it is now assumed for further evaluation that:

$$\nu^{\mathrm{Pb}},\nu^{\mathrm{Sn}} \sim \frac{1}{r_n^6} \tag{3.14}$$

which leads to roughly:

$$a^\alpha : a_1^\beta : a_3^\beta = 1.5:1:14. \tag{3.15}$$

It should explicitly be pointed out that it is this difference in surface tension data which leads to the formation of eutectic lamellae.

- In the very early stages of the phase separation the interfaces of the tin and lead rich regions will be coherent. However, when the equilibrium concentrations are approached the huge differences in the lattice constants between lead and tin (cf., Eq. (3.10)) will only permit incoherent interfaces to exist. Raghavan and Cohen (1975), p. 77, report that the specific surface energy, $\gamma$, of incoherent interfaces is in the range of:

$$\gamma \approx 0.5\text{–}1.5\ \mathrm{N/m} \tag{3.16}$$

the maximum value of which was used for the simulations. In order to relate this information on specific surface energy, $\gamma$, to the coefficients $a^\alpha$, $a_1^\beta$, $a_3^\beta$, of Eq. (3.15) the following definition is used (see also McFadden et al., 1993, p. 2017, and Appendix A):

$$2\gamma O = \int_V \kappa_{ij}^1 \frac{\partial^2 c}{\partial x_i \partial x_j}\,\mathrm{d}V = \int_V \frac{\partial}{\partial x_i}\left(\kappa_{ij}^1 \frac{\partial c}{\partial x_j}\right)\mathrm{d}V - \int_V \frac{\partial \kappa_{ij}^1}{\partial x_i}\frac{\partial c}{\partial x_j}\,\mathrm{d}V$$

$$= \oint_O N_i \kappa_{ij}^1 \frac{\partial c}{\partial x_j}\,\mathrm{d}A - \int_V \frac{\partial \kappa_{ij}^1}{\partial x_i}\frac{\partial c}{\partial x_j}\,\mathrm{d}V, \tag{3.17}$$

where $V$ is the volume surrounded by the interface $O$, the normal unit vector of which is given by $N_i$. As customary, the surface integral will be neglected in a large crystal. To evaluate the remaining part we put similarly to Eqs. (2.5) and (2.7)–(2.9):

$$\kappa_{ij}^1 = \kappa_{ij}^\beta - \frac{c^\beta - c}{c^\beta - c^\alpha}\left(\kappa_{ij}^\beta - \kappa_{ij}^\alpha\right) = -\left[\bar{\kappa}_{ij}^\beta - \frac{c^\beta - c}{c^\beta - c^\alpha}\left(\bar{\kappa}_{ij}^\beta - \bar{\kappa}_{ij}^\alpha\right)\right]c, \tag{3.18}$$

where it was defined (see Eqs. (A35) and (A36)):

$$\kappa\bar{\kappa}_{ij}^\alpha = \frac{1}{2}\omega\lambda^2\delta_{ij}, \quad k\bar{\kappa}_{ij}^\beta = \frac{1}{2}\omega\begin{bmatrix}\lambda_a^2 & 0 & 0\\ 0 & \lambda_a^2 & 0\\ 0 & 0 & \lambda_b^2\end{bmatrix}. \tag{3.19}$$

Consequently,

$$\frac{\partial \kappa_{ij}^1}{\partial x_i} = -\frac{\partial c}{\partial x_i}\left[\bar{\kappa}_{ij}^\beta - \frac{c^\beta - ac}{c^\beta - c^\alpha}\left(\bar{\kappa}_{ij}^\beta - \bar{\kappa}_{ij}^\alpha\right)\right]. \tag{3.20}$$

For further numerical evaluation it is now assumed that the second part in the bracket can be

neglected, i.e., the properties of the $\alpha$- and $\beta$-phase are supposed to be similar, and, moreover, isotropy is assumed (see Eq. (A35)):

$$\frac{\partial \kappa_{ij}^{1}}{\partial x_i} = -a\frac{\partial c}{\partial x_i}\delta_{ij}. \tag{3.21}$$

Hence, the following relation is obtained:

$$\gamma = \frac{a}{2O}\int_V \left(\frac{\partial c}{\partial x_i}\right)^2 \mathrm{d}V. \tag{3.22}$$

Next, it is assumed that the concentration gradient within the interface is linear and that equilibrium concentrations, $c^{\alpha}$ and $c^{\beta}$, have been reached within and outside of $V$. Then the following relation is easily derived:

$$a = 2\gamma\frac{\Delta x}{c^{\beta} - c^{\alpha}}. \tag{3.23}$$

For the numerical computations the width of the interface, $\Delta x$, was taken to be 50 atomic distances, i.e., in view of Eq. (3.10) roughly 25 nm. Note that because of the form of the phase diagram shown in Fig. 2, the difference $c^{\beta} - c^{\alpha}$ and, consequently, the coefficient $a$ depends on temperature. The value computed according to Eq. (3.23) was chosen for the coefficient $a_1^{\beta}$ and the remaining two other coefficients were then related to it by means of Eq. (3.15).

### 3.2. Low vs. high temperature aging without mechanical effects

In this subsection all mechanical effects of the development of the microstructural development are excluded. In other words, the last term in the equation for the diffusion flux (2.38) is switched off completely. Figs. 6 and 7 show the temporal development of the microstructure of an originally homogeneous composition of SnPb with six slight concentric disturbances/fluctuations of the eutectic concentration at 61.9%. The initial configuration is shown in Fig. 5. All morphology sequences shown

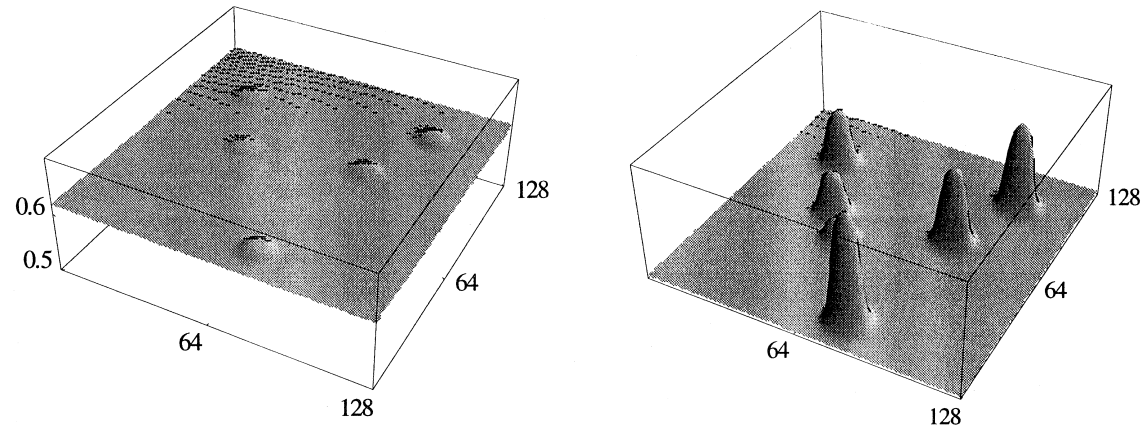


Fig. 5. Initial condition (the picture on the right is a magnified version of the picture on the left).

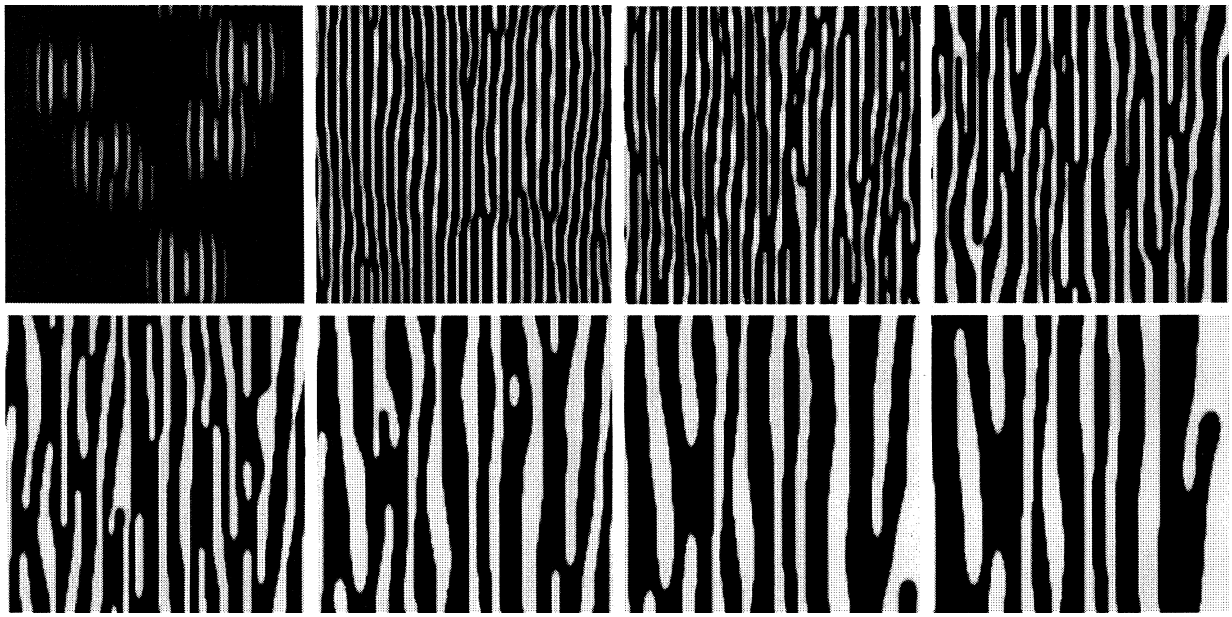

Fig. 6. Quenching from 183°C to 150°C, no mechanical contributions.

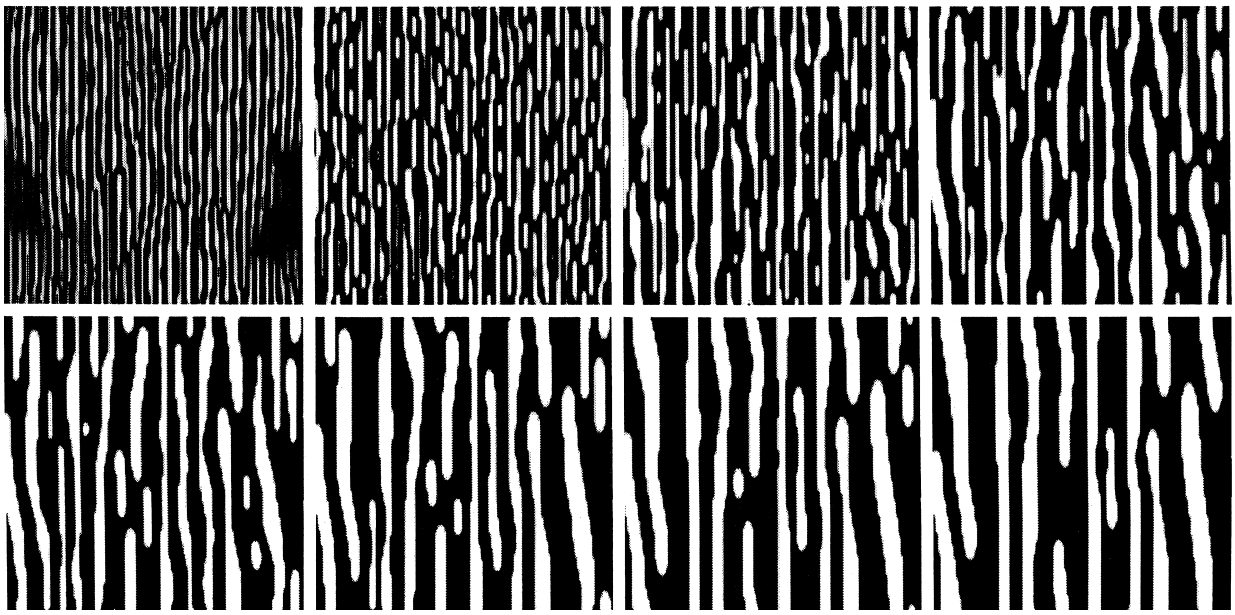

Fig. 7. Quenching from 183°C to 20°C, no mechanical contributions.

in this paper refer to 0.05, 0.1, 0.25, 0.5, 1.0, 2.5, 5.0 and 10.0 time units. The time-step chosen was $10^{-4}$ and the dimensions of the RVE are roughly 1.5 μm. This composition is quenched from 183°C down to the high and low temperature levels of Eqs. (3.5) and (3.6), respectively. A thickening of the lamellae which is characteristic to the eutectic composition is clearly visible. It also appears that the lamellae are slightly thicker for the higher temperature.

To a certain degree this behavior can be linked to experimental observations. Fig. 8 shows micrographs from the work of Harris et al. (1991). According to these the lamellae thicken at room temperature as well as at elevated temperature levels. They are clearly thicker in the high temperature case. Also, when compared to the numerical simulation, the characteristic dimensions, such as spacing or thickness, differ by an order of magnitude. This is clearly due to the insufficient knowledge of the material parameters which were used during the simulation. It should also be noted that the experimental pictures exhibit all effects, in particular, the influence of thermo-mechanical stresses. Moreover, an experiment is always three-dimensional which might also explain some of the discrepancies.

However, it can clearly be stated that the development of lamellae in the numerical simulation is due to the use of an anisotropic surface tension according to Eq. (3.15). If the same factor 1.5 is used for all directions and all phases, the microstructural development is clearly more isotropic as shown in the sequence of Fig. 9.

The sequence in Fig. 10 simulates the effect of thermal cycling on SnPb solder. The two rows show what happens if the temperature is changed from 20°C to 150°C (where the microstructure of the last

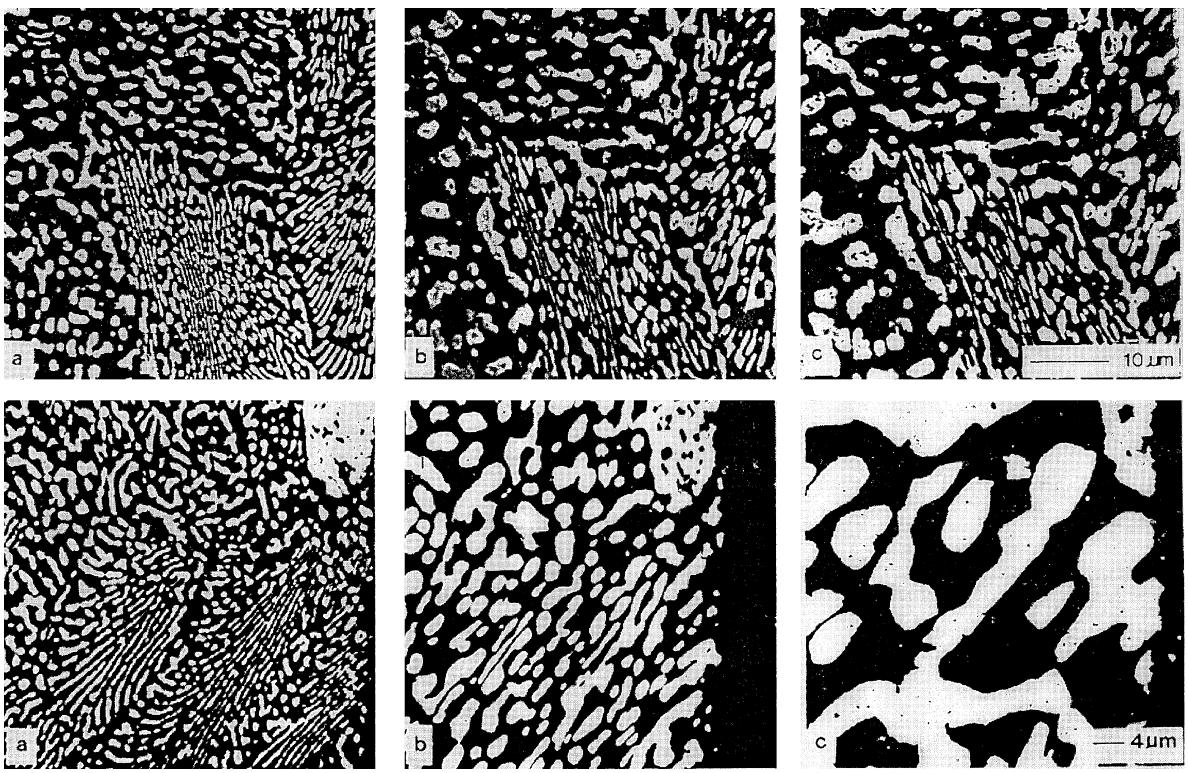


Fig. 8. Coarsening in a eutectic SnPb solder, top row: effect of room temperature aging after (a) 2 hours, (b) 17 days, and (c) 63 days after solidification; bottom row: (a) immediately after solidification, (b) after 3 hours at 125°C and (c) 300 hours at 125°C.

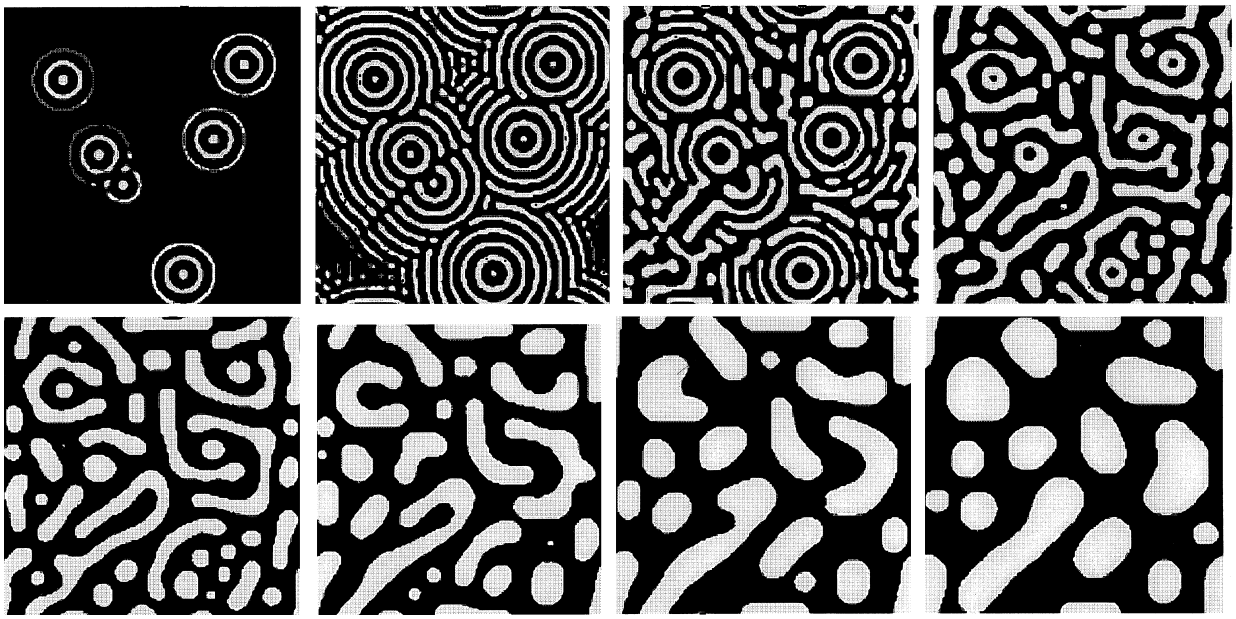

Fig. 9. Quenching from 183°C to 20°C, no mechanical contributions, isotropic surface tension.

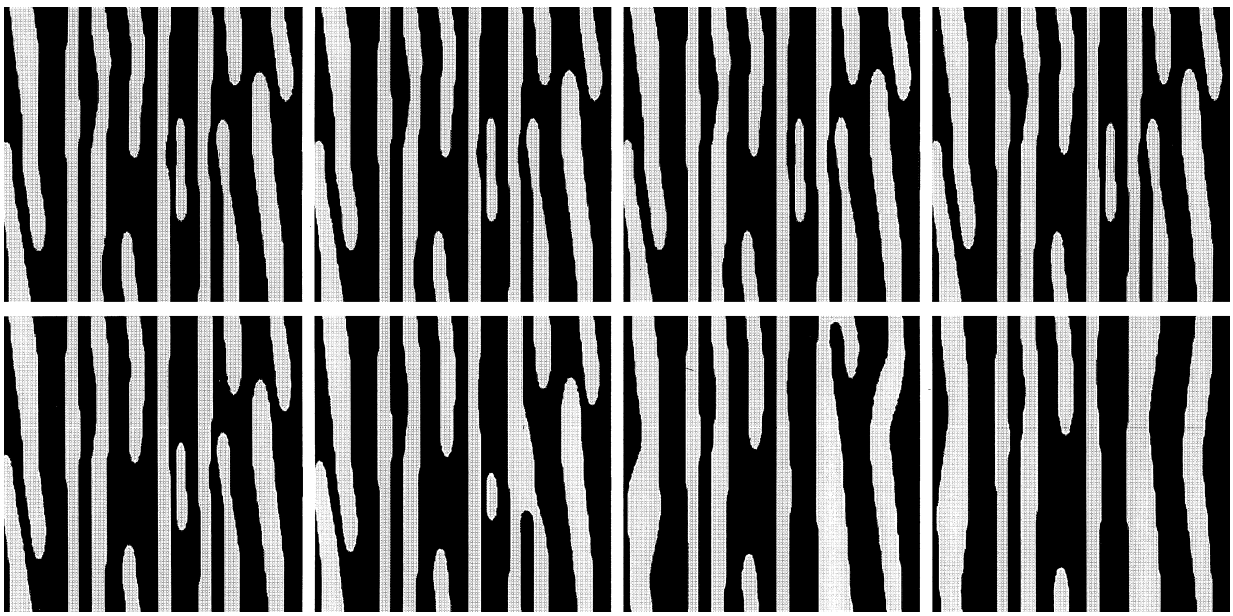

Fig. 10. Quenching from 20°C to 150°C, no mechanical contributions.

plot from Fig. 7 has been used as the initial condition). Obviously an increase in temperature leads to a further coarsening of the lamellae which, as further simulations show, seems to irreversibly remain and even increases slightly after cooling to the original starting point. However, this might depend on the duration of the hold time, and it is certainly also affected by the presence of external loads, as will be shown in the next subsection.

### 3.3. Low vs. high temperature aging with mechanical effects

The sequence in Fig. 11 is the same as in Fig. 6 but with thermal stresses. No external loads were applied. The difference between them is not very large. The lamellae in Fig. 11 appear slightly thicker. Whether this means that the chosen set of material parameters for the thermal stresses is incorrect and, if so, in which way it has to be corrected, or how the model must be modified is hard to decide since the thermal mismatch between the phases cannot be eliminated during an experiment. A possible way of how to get a better grip at this problem is to run aging experiments with other types of solders the phases of which should have different thermal expansion as well as stiffnesses. If the same type of thermal stress model would then be applied to describe their coarsening there is hope that by a relative comparison a decision could be made. It should also be mentioned that even though additional strain gradient terms are listed in the Appendix A they were, up to now, not considered in the simulations. These will be closer examined in a forthcoming paper by the authors.

Fig. 12 presents a sequence of simulated micrographs where in addition to the thermal loads an additional external load of $5\psi_0$ has been applied in horizontal direction. For binary alloys $\psi_0$ is typically in the order of 100 MPa. Hence, absolutely speaking, the load could be as high as 500 MPa which could not be supported by a SnPb solder. Indeed, further experimental research seems necessary to clarify this issue. However, for the time being the simulation shows that, provided they are sufficiently high, external stresses have an influence on the development of the microstructure of SnPb solder. In the

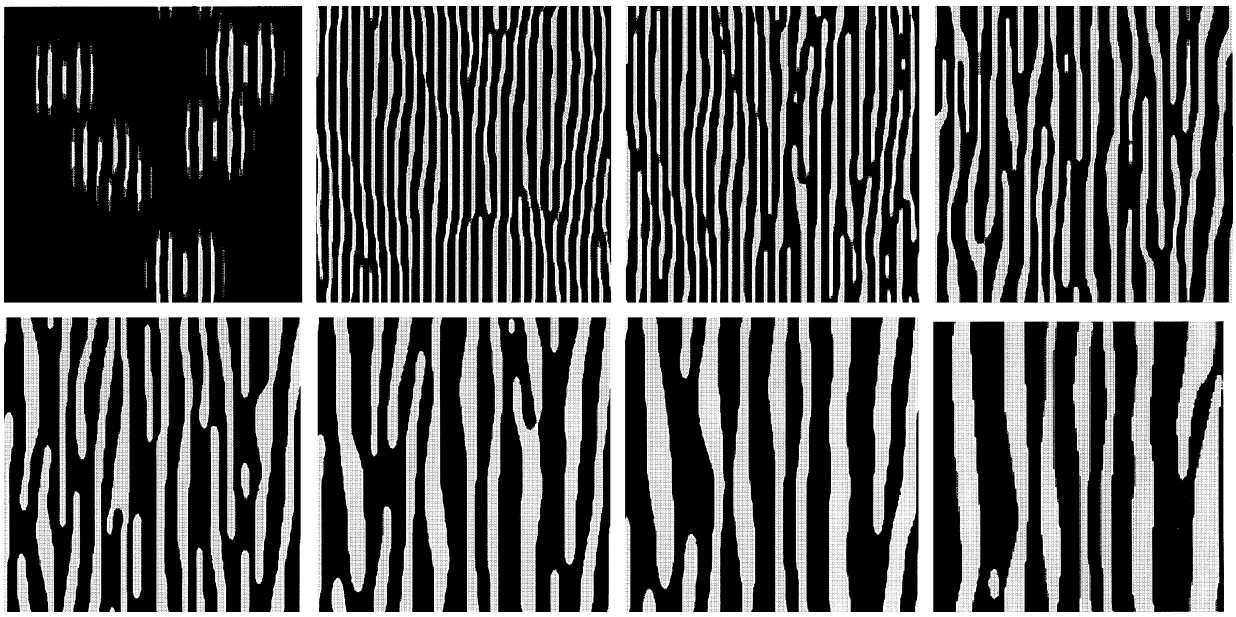

Fig. 11. Quenching from 183°C to 150°C, thermal stresses, no external loads.

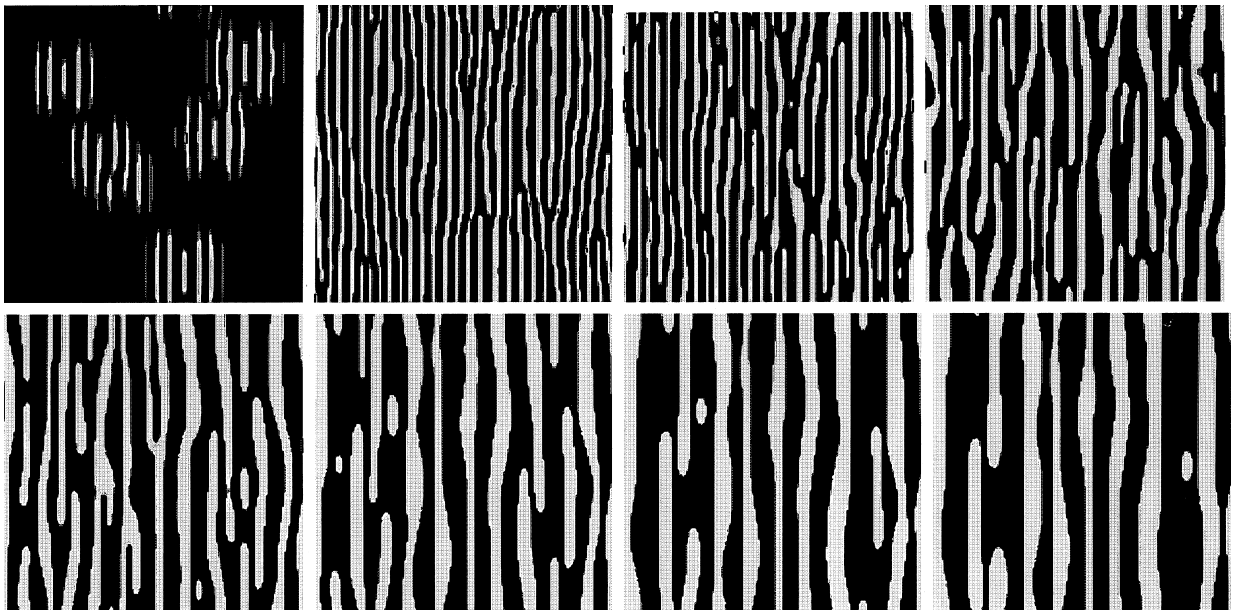

Fig. 12. Quenching from 183°C to 150°C, thermal stresses, external load $5\psi_0$ in horizontal direction.

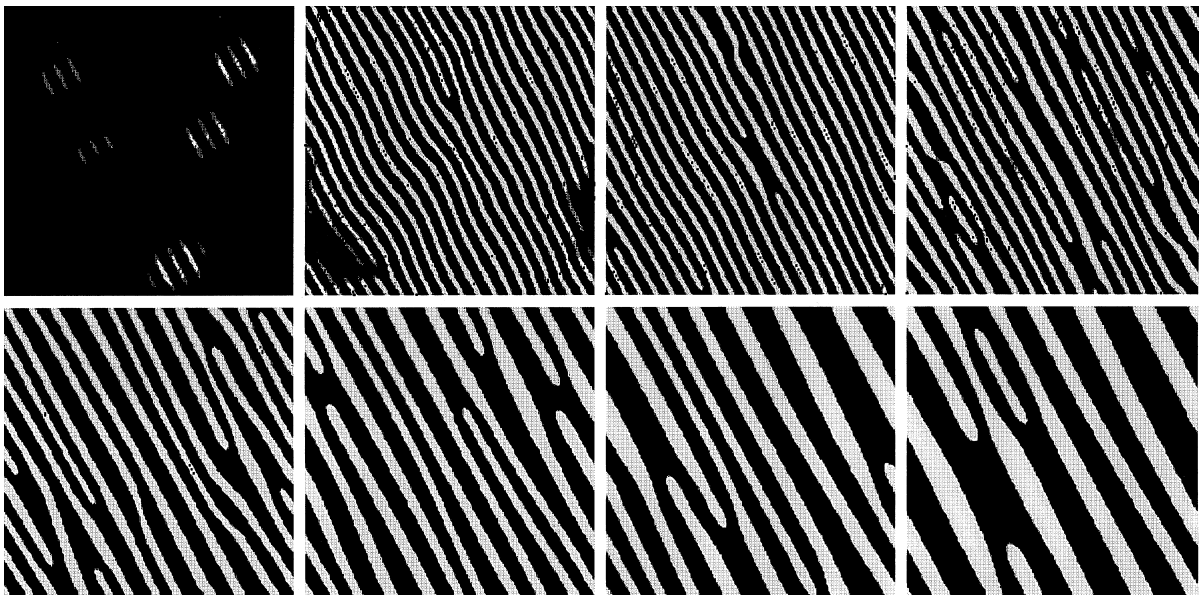

Fig. 13. Eutectic structure at an angle of 30° with respect to the main crystallographic axes.

present case they tend to thicken and misalign the lamellae at certain points. A certain delay in the evolution of a regular lamella structure can also be observed.

### 3.4. Misalignment with respect to the main crystallographic axes

The sequence of Fig. 13 is presented to show that the presented method is capable to simulate a eutectic SnPb lamella-structures which is not parallel to the main crystallographic axes. In fact, it should be possible to model differently oriented grain regions. However, in view of the insufficient knowledge regarding many material parameters this should become a second step toward the perfection of the modeling of solders.

## 4. Conclusions

The following issues were discussed in this paper:

- A purely continuum model can be devised and used to describe phase separation processes on a micro-morphological scale that are driven by diffusion through temperature, surface tensions, as well as local thermo-mechanical stresses and strains.
- This model has been successfully used for a qualitative modeling of the phase separation and coarsening process in binary eutectic SnPb solders that are subjected to change in temperature and external as well as internal mechanical stresses.
- Arguments on the atomic scale can be used to gain additional information on material quantities such as the relative ranking of the components of the tension of surface tensions.
- The entropy principle can be used, together with atomistic arguments, to rationally derive the appropriate expressions for the stress-coupled diffusion flux.
- Discrete Fourier transforms can most effectively be used to solve mechanical as well the diffusion problems encountered during changes of micro-morphology. The corresponding theory was outlined and applied to the case of eutectic SnPb solders.

## Acknowledgements

The foundations to this paper were laid during two visits of W. Dreyer to the Department of Mechanical and Chemical Engineering at Heriot-Watt University and of W.H. Müller to the Weierstraß Institute in the summer of 1998. Their stays were financially supported by Heriot-Watt University and by the British Council.

## Appendix A. A modicum of thermodynamics

In this paper the following field variables are of primary interest:
motion:

$$x_i = \tilde{x}_i(X_k,t), \quad i,j \in \{1,2,3\}, \tag{A1}$$

the concentrations of all constituents of the mixture:

$$c^A = \frac{\tilde{\rho}_0^A(X_k,t)}{\tilde{\rho}_0(X_k,t)}, \tag{A2}$$

the temperature:

$$T = \tilde{T}(X_k,t). \tag{A3}$$

The symbols $X_k$ indicate the material coordinates of a continuum particle, $t$ denotes the time, the subscript $A$ identifies the constituent, and $\rho_0^A$ and $\rho_0$ are the mass densities with respect to the reference configuration of constituent $A$ and of the total mass, respectively. The following relations hold for the current total mass density, $\rho$, and for the current partial mass densities, $\rho^A$ (Müller, 1985, p. 61, p. 71):

$$\rho = \frac{\rho_0}{\det \underline{F}}, \quad \rho = \sum_A \rho^A, \tag{A4}$$

where $\underline{F}$ denotes the deformation gradient:

$$F_{ij} = \frac{\partial \tilde{x}_i}{\partial X_j}. \tag{A5}$$

Sometimes it happens that the solid in the reference configuration consists already of two phases, $\alpha$ and $\beta$. In this case we write:

$$\rho_0 = \rho_0^\beta - \left(\rho_0^\beta - \rho_0^\alpha\right)\tilde{\theta}(X_k,t), \tag{A6}$$

with:

$$\tilde{\theta}(X_k,t) = \frac{c^\beta - \tilde{c}(X_k,t)}{c^\beta - c^\alpha}. \tag{A7}$$

Within this section on thermodynamics the right Cauchy–Green tensor, $C_{ij}$, is used as a general strain measure instead of the infinitesimal strain, $\varepsilon_{ij}$:

$$C_{ij} = F_{ki}F_{kj} \approx 1 + 2\varepsilon_{ij} \quad \text{for } |\varepsilon_{ij}|. \tag{A8}$$

The solution for the field variables is based on the balance equations for the concentration, $c$:[7]

$$\rho_0 \dot{c} + \frac{\partial J_k}{\partial X_k} = 0, \tag{A9}$$

momentum:

$$\rho_0 \dot{\mathrm{v}}_i - \frac{\partial t_{ik}}{\partial X_k} = 0, \tag{A10}$$

and for internal energy, $u$:

$$\rho_0 \dot{u} + \frac{\partial Q_k}{\partial X_k} = t_{ik}\frac{\partial \mathrm{v}_i}{\partial X_k} \equiv \frac{1}{2} T_{ij}\dot{C}_{ij}. \tag{A11}$$

[7] For simplicity a binary mixture with no chemical reactions was assumed and the index $A$ is omitted from now on.

In these equations dots refer to material time derivatives, $J_k$ denotes the diffusion flux, $t_{ik}$ and $T_{ij}$ are the first and second Piola–Kirchhoff stress tensors, respectively, and $Q_k$ is the material heat flux (Müller, 1985, p. 77). If the differences between the current and the reference configuration are ignored, as it is customary for small deformations and as it was done during the simulations presented in this paper, there is no difference between $t_{ik}$ and $T_{ij}$, and both tensors can be approximated by the Cauchy stress tensor, $\sigma_{ij}$.

Note that in the simulations presented in this paper the acceleration terms, $\rho_0 \dot{v}_i$, in the balance of momentum were neglected and the balance of internal energy was completely ignored since the temperature field was prescribed as constant and homogeneous throughout the solder.

The balance equations become field equations if the quantities $J_i$, $T_{ij}$ (or $t_{ij}$), $u$, and $Q_i$ are related to the variables in a material-dependent manner by constitutive equations. Restrictions for such equations are imposed by the local inequality for the entropy, $s$, which reads (Müller, 1985, p. 168):

$$\rho_0 \dot{s} + \frac{\partial \phi_k}{\partial X_k} = \Sigma \geq 0, \tag{A12}$$

where $\phi_k$ is the entropy flux and $\Sigma$ denotes the (positive) entropy production density which are also constitutive quantities, in the same manner as $J_i$, etc.

Note that this inequality holds exclusively for solutions of the field equations. These constraints are taken into account in the famous lemma by I-Shih Liu and Müller (see Müller, 1985, p. 167) which allows for a straightforward derivation of all the restrictions imposed by the entropy principle on the constitutive relations. It states that if the entropy inequality (A12) holds only for solutions of the field equations then:

$$\rho_0 \dot{s} + \frac{\partial \phi_k}{\partial X_k} - \Lambda^c \left( \rho_0 \dot{c} + \frac{\partial J_k}{\partial X_k} \right) - \Lambda_i^{\mathrm{v}} \left( \rho_0 \dot{v}_i - \frac{\partial t_{ik}}{\partial X_k} \right) - \Lambda^u \left( \rho_0 \dot{u} + \frac{\partial Q_k}{\partial X_k} - \frac{1}{2} T_{ij} \dot{C}_{ij} \right) \geq 0 \tag{A13}$$

must hold for arbitrary fields of concentration, motion, and temperature. The symbols $\Lambda^c$, $\Lambda_i^{\mathrm{v}}$, $\Lambda^u$ are Lagrange multipliers which may depend on all independent variables including their derivatives. The inequality must now be exploited in order to arrive at reduced, preferably explicit, forms for $u$, $J_k$, $T_{ij}$, $Q_k$ in terms of the fields $c$, $\underline{C}$, $T$, and their derivatives.

The general exploitation of Eq. (A13) will be presented in another paper by the authors. It turns out that the effort during this exploitation can be reduced considerably if it is assumed, motivated by experience, that:

$$\Lambda^u = \frac{1}{T} > 0. \tag{A14}$$

Motivated by arguments from statistical mechanics (Cahn and Hilliard, 1958, p. 262) the specific free energy, $\psi = u - Ts$, of the binary alloy is a *known* function of the following variables:

$$\psi = \tilde{\psi} \left( c, \frac{\partial c}{\partial X_k}, \frac{\partial^2 c}{\partial X_k \partial X_s}, C_{ij}, \frac{\partial C_{ij}}{\partial X_k}, \frac{\partial^2 C_{ij}}{\partial X_k \partial X_s}, T \right). \tag{A15}$$

Consequently, the inequality is linear with respect to $\dot{v}_i$ and, therefore:

$$\Lambda_i^{\mathrm{v}} = 0 \tag{A16}$$

must hold since otherwise the inequality could easily be violated. Insertion of Eqs. (A14)–(A16) into Eq. (A13) and performing the differentiations yields:

$$\begin{aligned}
&\frac{\rho_0}{\Lambda^u}\left(s+\frac{\partial\psi}{\partial T}\right)\dot{\Lambda}^u-\rho_0\Lambda^u\left(\frac{\partial\psi}{\partial c}+\frac{\Lambda^c}{\Lambda^u}\right)\dot{c}-\rho_0\Lambda^u\left(\frac{\partial\psi}{\partial C_{ij}}-\frac{1}{2\rho_0}T_{ij}\right)\dot{C}_{ij}-\rho_0\Lambda^u\frac{\partial\psi}{\partial(\partial c/\partial X_k)}\left(\frac{\partial c}{\partial X_k}\right)^{\cdot}\\
&\quad-\rho_0\Lambda^u\frac{\partial\psi}{\partial\left(\partial C_{ij}/\partial X_k\right)}\left(\frac{\partial C_{ij}}{\partial X_k}\right)^{\cdot}\quad-\rho_0\Lambda^u\frac{\partial\psi}{\partial\left(\partial^2 c/\partial X_k\partial X_s\right)}\left(\frac{\partial^2 c}{\partial X_k\partial X_s}\right)^{\cdot}\\
&\quad-\rho_0\Lambda^u\frac{\partial\psi}{\partial\left(\partial^2 C_{ij}/\partial X_k\partial X_s\right)}\left(\frac{\partial^2 C_{ij}}{\partial X_k\partial X_s}\right)^{\cdot}+\frac{\partial\phi'_k}{\partial X_k}+Q_k\frac{\partial\Lambda^u}{\partial X_k}+J_k\frac{\partial\Lambda}{\partial X_k}\geq 0,
\end{aligned}\tag{A17}$$

with the definition:

$$\phi'_k=\phi_k-\Lambda^u Q_k-\Lambda^c J_k.\tag{A18}$$

With the same kind of argument as above the linearity in $\dot{\Lambda}^u$ implies:

$$s=-\frac{\partial\psi}{\partial T}.\tag{A19}$$

If the flux $\phi'_k$ is supposed to depend on the same variables as the free energy and all the other constitutive quantities then it can easily be shown that the free energy could only depend on $c$, $C_{ij}$, and $T$ and *not* on their derivatives. On the other hand, it is known from statistical mechanics that such a dependence exists. The simplest way to achieve consistency with the second law is to assume that:

$$\phi'_k=\varphi_k\dot{c}+\varphi_{kij}\dot{C}_{ij}+\varphi_{ks}\left(\frac{\partial c}{\partial X_s}\right)^{\cdot}+\varphi_{kijs}\left(\frac{\partial C_{ij}}{\partial X_s}\right)^{\cdot},\tag{A20}$$

where, in consistency with Eq. (A15), all coefficients $\varphi$ may show a functional dependence as follows:

$$\varphi=\tilde{\varphi}\left(c,\frac{\partial c}{\partial X_k},\frac{\partial^2 c}{\partial X_k\partial X_s},C_{ij},\frac{\partial C_{ij}}{\partial X_k},\frac{\partial^2 C_{ij}}{\partial X_k\partial X_s},T\right).\tag{A21}$$

If Eq. (A20) is now inserted into Eq. (A17) the following result is obtained:[8]

$$\begin{aligned}
&-\rho_0\Lambda^u\left(\frac{\partial\psi}{\partial c}+\frac{\Lambda^c}{\Lambda^u}-\frac{1}{\rho_0\Lambda^u}\frac{\partial\varphi_k}{\partial X_k}\right)\dot{c}-\rho_0\Lambda^u\left(\frac{\partial\psi}{\partial C_{ij}}-\frac{1}{2\rho_0}T_{ij}-\frac{1}{\rho_0\Lambda^u}\frac{\partial\varphi_{kij}}{\partial X_k}\right)\dot{C}_{ij}\\
&\quad+\left(\varphi_k+\frac{\partial\varphi_{ks}}{\partial X_k}-\rho_0\Lambda^u\frac{\partial\psi}{\partial(\partial c/\partial X_s)}\right)\left(\frac{\partial c}{\partial X_s}\right)^{\cdot}+\left(\varphi_{sij}+\frac{\partial\varphi_{kijs}}{\partial X_k}-\rho_0\Lambda^u\frac{\partial\psi}{\partial\left(\partial C_{ij}/\partial X_s\right)}\right)\left(\frac{\partial C_{ij}}{\partial X_s}\right)^{\cdot}\\
&\quad+\left(\varphi_{ks}-\rho_0\Lambda^u\frac{\partial\psi}{\partial\left(\partial^2 c/\partial X_k\partial X_s\right)}\right)\left(\frac{\partial^2 c}{\partial X_k\partial X_s}\right)^{\cdot}+\left(\varphi_{kijs}-\rho_0\Lambda^u\frac{\partial\psi}{\partial\left(\partial^2 C_{ij}/\partial X_k\partial X_s\right)}\right)\left(\frac{\partial^2 C_{ij}}{\partial X_k\partial X_s}\right)^{\cdot}\\
&\quad+Q_k\frac{\partial\Lambda^u}{\partial X_k}+J_k\frac{\partial\Lambda^c}{\partial X_k}\geq 0.
\end{aligned}\tag{A22}$$

[8] Because of their independence material time derivatives and spatial derivatives can simply be interchanged. This explains why a Lagrangian formulation was used.

The inequality (A22) is linear in $\dot{c}$, $\dot{C}_{ij}$, $(\frac{\partial c}{\partial X_s})\dot{}$, $(\frac{\partial C_{ij}}{\partial X_s})\dot{}$ and, following the same line of arguments as above, it follows that:

$$\Lambda^c = -\frac{1}{T}\frac{\partial \psi}{\partial c} + \frac{1}{\rho_0}\frac{\partial \varphi_s}{\partial X_s}, \tag{A23}$$

$$T_{ij} = 2\rho_0 \frac{\partial \psi}{\partial C_{ij}} - 2T\frac{\partial \varphi_{sij}}{\partial X_s}, \tag{A24}$$

$$\varphi_s = -\frac{\partial \varphi_{ks}}{\partial X_k} + \frac{\rho_0}{T}\frac{\partial \psi}{\partial(\partial c/\partial X_s)}, \tag{A25}$$

$$\varphi_{ks} = \frac{\rho_0}{T}\frac{\partial \psi}{\partial\left(\partial^2 c/\partial X_k \partial X_s\right)}, \tag{A26}$$

$$\varphi_{kij} = -\frac{\partial \varphi_{kijs}}{\partial X_k} + \frac{\rho_0}{T}\frac{\partial \psi}{\partial\left(\partial C_{ij}/\partial X_s\right)}, \tag{A27}$$

$$\varphi_{kijs} = \frac{\rho_0}{T}\frac{\partial \psi}{\partial\left(\partial^2 C_{ij}/\partial X_k \partial X_s\right)}. \tag{A28}$$

There remains the residual inequality:

$$Q_k \frac{\partial \Lambda^u}{\partial X_k} + J_k \frac{\partial \Lambda^c}{\partial X_k} \geq 0. \tag{A29}$$

If coupling between heat and diffusion is ignored the simplest way to satisfy Eq. (A29) is given by the choice:

$$Q_i = -\kappa_{ik}\frac{\partial T}{\partial X_k}, \tag{A30a}$$

$$J_i = \rho_0 M_{ik} T \frac{\partial \Lambda^c}{\partial X_k}, \tag{A30b}$$

with two positive definite matrices, one for the thermal conduction coefficients, $\kappa_{ik}$, and one for the mobility coefficients, $M_{ik}$. After elimination of $\varphi_k$, $\varphi_{ks}$, $\varphi_{kij}$, and $\varphi_{kijs}$ it follows that:

$$\begin{aligned}\Lambda^c = &-\frac{1}{T}\frac{\partial \psi}{\partial c} + \frac{1}{T}\frac{\partial}{\partial X_k}\left(\frac{\partial \psi}{\partial(\partial c/\partial X_k)}\right) + \frac{1}{\rho_0}\frac{\partial \psi}{\partial(\partial c/\partial X_k)}\frac{\partial}{\partial X_k}\left(\frac{\rho_0}{T}\right) \\ &- \frac{1}{T}\frac{\partial^2}{\partial X_k \partial X_s}\left(\frac{\partial \psi}{\partial\left(\partial^2 c/\partial X_k \partial X_s\right)}\right) - \frac{1}{\rho_0}\frac{\partial \psi}{\partial\left(\partial^2 c/\partial X_k \partial X_s\right)}\frac{\partial^2}{\partial X_k \partial X_s}\left(\frac{\rho_0}{T}\right),\end{aligned} \tag{A31}$$

$$T_{ij} = 2\rho_0 \frac{\partial \psi}{\partial C_{ij}} - 2\rho_0 \frac{\partial}{\partial X_k}\left(\frac{\partial \psi}{\partial\left(\partial C_{ij}/\partial X_k\right)}\right) - T\frac{\partial \psi}{\partial\left(\partial C_{ij}/\partial X_k\right)}\frac{\partial}{\partial X_k}\left(\frac{\rho_0}{T}\right)$$
$$+ 2\rho_0 \frac{\partial^2}{\partial X_k \partial X_s}\left(\frac{\partial \psi}{\partial\left(\partial^2 C_{ij}/\partial X_k \partial X_s\right)}\right) + 2T\frac{\partial \psi}{\partial\left(\partial^2 C_{ij}/\partial X_k \partial X_s\right)}\frac{\partial^2}{\partial X_k \partial X_s}\left(\frac{\rho_0}{T}\right). \tag{A32}$$

Thus, the diffusion flux as well as the stress, which are the quantities of primary interest in this paper, are reduced to derivatives of the free energy alone. For the simulations discussed in this paper Eqs. (A30b), (A31), and (A32) are the most important results of this section on thermodynamics. The reference configuration is often identified with the melt. For that choice the various $\rho_0$-terms in Eqs. (A31) and (A32) drop out if, in addition, a homogeneous temperature distribution is assumed.

Following the statistical arguments present on p. 263 of the paper by Cahn and Hilliard (1958), the following form of the specific free energy can be established if coupling between strain and concentrations on the micro-scale is ignored:

$$\psi = \psi' + \kappa^1_{ij}\frac{\partial^2 c}{\partial X_i \partial X_j} + \frac{1}{2}\kappa^2_{ij}\frac{\partial c}{\partial X_i}\frac{\partial c}{\partial X_j}. \tag{A33}$$

In here $\psi'$ is the configurational part of the free energy, which still includes strain ('elastic') energy, and the coefficients $\kappa^1_{ij}$ and $\kappa^2_{ij}$ are given by:

$$\kappa^2_{ij} = 0, \tag{A34}$$

$$\kappa^1_{ij} = a\delta_{ij}, \quad a = -\frac{1}{2}\omega\lambda^2 c \text{ (for cubic crystals)}, \tag{A35}$$

and:

$$\kappa^1_{ij} = \begin{pmatrix} a & 0 & 0 \\ 0 & a & 0 \\ 0 & 0 & b \end{pmatrix}, \quad a = -\frac{1}{2}\omega\lambda_a^2 c,\ b = -\frac{1}{2}\omega\lambda_b^2 c \text{ (for tetragonal crystals)}, \tag{A36}$$

where:

$$\omega = \sum_n Z_n \nu_n, \quad \nu_n = E_{AB} - \frac{1}{2}(E_{AA} + E_{BB}), \quad \lambda^2 = \frac{1}{3\omega}\sum_n Z_n r_n^2 \nu_n, \tag{A37}$$

$$\lambda_a^2 = \frac{1}{2\omega}\sum_n \left(Z_n - \sum_{\alpha=1}^{Z_n}\cos^2(\vartheta^\alpha)\right) r_n^2 \nu_n, \quad \lambda_b^2 = \frac{1}{\omega}\sum_n \left(\sum_{\alpha=1}^{Z_n}\cos^2(\vartheta^\alpha)\right) r_n^2 \nu_n. \tag{A38}$$

Moreover, $Z_n$ is the coordination number of the $n$th coordination shell at a radius $r_n$ from a reference atom, $E_{AA}$, $E_{BB}$, and $E_{AB}$ denote the pairwise interaction potentials of a binary alloy, and $\vartheta^\alpha$ is the azimuthal angle which starts from the tetragonal axis. If the temperature within the alloy is homogeneous and if the reference configuration is chosen to be the one of the melt, insertion of Eq. (A33) into Eq. (A34) leads to the following result for the diffusion flux of Eq. (A30b):

$$J_i = -\rho_0 M_{ij}\frac{\partial}{\partial X_j}\left(\frac{\partial \psi'}{\partial c} + \frac{\partial \kappa^1_{rs}}{\partial c}\frac{\partial^2 c}{\partial X_r \partial X_s} + \frac{\partial^2 \kappa^1_{rs}}{\partial X_r \partial X_s}\right) = -\rho_0 M_{ij}\frac{\partial}{\partial X_j}\left(\frac{\partial \psi'}{\partial c} - a_{rs}\frac{\partial^2 c}{\partial X_r \partial X_s}\right), \tag{A39}$$

where

$$a_{ij} = \omega\lambda^2\delta_{ij} \quad \text{(for cubic crystals)}, \tag{A40}$$

and

$$a_{ij} = \omega\begin{pmatrix} \lambda_a^2 & 0 & 0 \\ 0 & \lambda_a^2 & 0 \\ 0 & 0 & \lambda_b^2 \end{pmatrix} \quad \text{(for tetragonal crystals)}. \tag{A41}$$

In the simulations presented in this paper the contribution of strain gradients was neglected. Thus, the configurational part of the free energy, $\psi'$, is additively split into a strain free configurational part, $\psi_0$, and another part, $\psi_{\text{def}}$, which contains the free energy stored due to the deformation, $C_{ij}$:

$$\psi' = \tilde{\psi}_0(c) + \tilde{\psi}_{\text{def}}\big(c, C_{ij}\big). \tag{A42}$$

For a linear elastic body which is subjected to small deformations we write:

$$\psi_{\text{def}} = \frac{1}{2}\big(\varepsilon_{ij} - \varepsilon^*_{ij}(c)\big)C_{ijkl}(c)\big(\varepsilon_{kl} - \varepsilon^*_{kl}(c)\big), \quad \text{where } \varepsilon^*_{kl}(c) = \alpha_{kl}(c)\Delta T, \tag{A43}$$

which, together with Eq. (A39), explains the form of the diffusion flux shown in Eq. (2.38).

Experiments on solder materials indicate that the stress fields have an observable influence on diffusion. However, if the influence on stresses is described in terms of (A43) extremely high stresses are necessary to simulate this influence. In an upcoming publication by the authors it is intended to also consider the influence of deformation gradients.

## References


Albrecht, H.-J., Gamalski, J., 1996. Fatigue properties of BGA solder joints: a comparison of thermal and power cycle tests. In: Proc. SMI '96, San Jose, 61–80.

Cahn, J.W., Hilliard, J.E., 1958. Free energy of a non-uniform system. Part I: Interfacial free energy. The Journal of Chemical Physics 28 (1), 258–267.

Callister Jr, W.D., 1997. Materials Science and Engineering: An Introduction. Wiley, New York.

Canuto, C., Hussaini, M.Y., Quateroni, A., Zang, T.A., 1988. Spectral methods in fluid dynamics. Springer Series in Computational Physics. Springer Verlag, New York.

Chen, L.-Q., Wang, Y., Khachaturyan, A.G., 1991. Transformation-induced elastic strain effect on the precipitation kinetics of ordered intermetallics. Philosophical Magazine Letters 64 (5), 241–251.

Darveaux, R., Banerji, K., Mawer, A., Dody, G., 1995. Reliability of plastic ball grid array assembly. In: Lau, J.H. (Ed.), Ball Grid Array Technology. SMTnet, pp. 380–442.

de Fontaine, D. 1975. Clustering effect in solid solutions. In: Hannah, N.B. (Ed.), Treatise on Solid State Chemistry. Plenum Press, New York, London, pp. 129–178.

Dreyer, W., 1994. Development of microstructure based viscoplastic models for an advanced design of single crystal hot section components. In: Olschewski, J. (Ed.), Development of Microstructural Based Viscoplastic Models for an Advanced Design of Single Crystal Hot Section Components. Brite/Euram Per. Prog. Rpt., pp. A.1-17–A.1-29.

Dreyer, W., Müller, W.H., Olschewski, J., 1998. An approximate analytical 2D-solution for the stresses and strains in eigenstrained cubic materials. Acta Mechanica, in press.

Falk, G., 1966. Theoretische Physik auf der Grundlage einer allgemeinen Dynamik, Band I a Aufgaben und Ergänzungen zur Punktmechanik. Springer, Berlin, Heidelberg, New York.

Hacke, P.L., Sprecher, A.F., Conrad, H., 1997. Microstructure coarsening during thermo-mechanical fatigue of PbSn solder joints. Journal of Electronic Materials 28 (7), 774–782.

Handbook of Chemistry and Physics, 1995. 76th ed. CRC, The Chemical Rubber Co., Cleveland, OH.

Harris, P.G., Chaggar, K.S., Whitmore, M.A., 1991. The effect of ageing on the microstructure of 60 : 40 tin–lead solders. Soldering and Surface Mount Technology 7, 20–23.

Hauck, T., Müller, W.H., Albrecht, H.-J., Gamalski, J., 1996. Concepts Toward Lifetime Analysis of BGA Structures. In: Proc. Surface Mount International San Jose, vol. 1, 109–120.

Hawick, K.A., 1991. Domain growth in alloys. Ph.D. thesis, Edinburgh University.

Hwang, J.S., Lucey, G., 1993. Strengthened solder materials for electronic packages. In: Proceedings of the Surface Mount International, 662–676.

Flanders, D.R., Jacobs, E.G., Pinizotto, R.F., 1997. Activation energies of intermetallic growth of Sn–Ag eutectic solder on copper substrates. Journal of Electronic Materials 26 (7), 883–887.

Jendrny, J., Müller, W.H., Albrecht, H.-J., 1997. Strength and lifetime analysis of SMT solder joints: An exemplary study of the MiniMelf component. In: Proc. Surface Mount International Conference, San Jose, 626–636.

Khachaturyan, A.G., Semenovskaya, S., Tsakalakos, T., 1995. Elastic strain energy of inhomogeneous solids. Physical Review B 52 (22), 15909–15919.

Koyama, T., Miyazaki, T., 1994. Computer simulation of phase decomposition in real alloy systems. In: Johnson, W.C., Howe, J.M., Laughlin, D.E. (Eds.), Solid → Solid Phase Transformations. The Minerals, Metals and Materials Society, Warrendale, Pennsylvania, 15086, pp. 365–370.

Koyama, T., Miyazaki, T., 1998. Computer simulation of phase decomposition in two dimensions based on a discrete type non-linear diffusion equation. Materials Transactions, JIM 39 (1), 169–178.

Koyama, T., Miyazaki, T., Mebed, A.E.-A.M., 1994. Computer simulations of phase decomposition in real alloy systems based on the modified Khachaturyan diffusion equation. Metallurgical and Materials Transactions A 26A, 1995–2617.

Koyama, T., Miyazaki, T., Doi, M., Mebed, A.E.-A.M., Moriya, T., 1996. Computer simulation of phase decomposition in Fe–Mo alloy based on discrete type diffusion equation. J. Japan. Inst. Metals 60 (6), 560–568.

Küpper, T., Masbaum, N., 1994. Simulation of particle growth and Ostwald ripening via the Cahn–Hilliard equation. Acta Metall. Mater 42 (6), 1847–1858.

Laberge, C.A., Fratzl, P., Lebowitz, J.L., 1997. Microscopic model for directional coarsening of precipitates in alloys under external load. Acta. Mater 45 (10), 3949–3961.

Lau, J.H., Rice, D.W., 1985. Solder joint fatigue in surface mount technology: state of the art. Solid State Technology, 91–104.

Lee, J.A., Raynor, G.V., 1955. The lattice spacings of binary tin-rich alloys. Proc. Phys. Soc. LXVII 10-B, 737–747.

Li, D.Y., Chen, L.-Q., 1997. Computer simulation of morphological evolution and rafting of particles in Ni-based superalloys under applied stress. Scripta Materialia 37 (9), 1271–1277.

Logsdon, W.A., Liaw, P.K., Burke, M.A., 1990. Fracture behavior of 63Sn–37Pb solder. Engineering Fracture Mechanics 36 (2), 183–218.

Massalski, T.B. 1965. Structure of solid solutions. In: Cahn, R.W. (Ed.), Physical Metallurgy. North-Holland, Amsterdam, pp. 149–211.

McCormack, M., Khachaturyan, A.G., Morris Jr, J.W., 1992. A two-dimensional analysis of the evolution of coherent precipitates in elastic media. Acta Metall. Mater 40 (2), 325–336.

McFadden, G.B., Wheeler, A.A., Braun, R.J., Coriel, S.R., 1993. Phase-field models for anisotropic interfaces. Physical Review E 48 (3), 2016–2024.

Mebed, A.M., Koyama, T., Miyazaki, T., 1997. Computer simulation of A2/B2 second-order phase transition based upon the Khachaturyan diffusion equation. Journal of Materials Science 32, 5797–5804.

Miyazaki, T., Koyama, T., 1996. Theoretical analysis of phase decomposition in real alloy systems based on the non-linear diffusion equation. Materials Transactions, JIM 37 (4), 684–690.

Miyazaki, T., Koyama, T., 1997. Computer simulation of microstructure formation of the real alloy systems based on the discrte type non-linear diffusion equation. In: Sugiyama, M. (Ed.), Proceedings of the Workshop 'Recent Developments in the Study of Irreversible Processes', 18–19 September 1997. Nagoya Institute of Technology, pp. 79–85.

Miyazaki, T., Takeuchi, A., Koyama, T., Kozakai, T., 1991. Computer simulation of phase decomposition in the regular solid solution based upon the Chan–Hilliard's non-linear diffusion equation. Materials Transactions, JIM 32 (10), 915–920.

Moulinec, H., Suquet, P., 1994. A fast numerical method for computing the linear and nonlinear mechanical properties of composites. C. R. Acad. Sci. Paris 318 (2), 1417–1423.

Moulinec, H., Suquet, P., 1997. A numerical method for computing the overall response of nonlinear composites with complex microstructure. Comp. Meth. Appl. Mech. Engng., 69–87.

Müller, I., 1992. Thermodynamics. Pitman, Boston, London, Melbourne.

Müller, W.H., 1996. Mathematical vs. experimental stress analysis of inhomogeneities in solids. Journal de Physique IV. Colloque C1, supplément au Journal de Physique III 6, C1-139–C1-148.

Müller, W.H., 1998a. Fourier transforms and their application to the formation of textures and changes of morphology in solids. In: Proc. IUTAM Symp. on Transformation Problems in Composite and Active Materials, Cairo, 61–72.

Müller, W.H., 1998b. The possibilities of Fourier transforms for the calculation of damage evolution in metals. ZAMM, 78(52) 5637–5640.

Müller, W.H., Neumann, S., 1998. An approximate analytical 3D-solution for the stresses and strains in eigenstrained cubic materials. Int. J. Sol. Struct 35 (22), 2931–2958.

Mura, T., 1987. Micromechanics of Defects in Solids, 2nd ed. Martinus Nijhoff, Dordrecht, The Netherlands.

Nishimori, H., Onuki, A., 1990. Pattern formation in phase-separating alloys with cubic symmetry. Physical Review B 42 (1), 980–983.

Nylen, M., Hutchinson, B., Gustavsson, U., 1997. Microstructural degradation of solder. In: Proc. Micro Materials, Micro Mat '97, Berlin, 890–895.

Ozmat, B., 1990. A nonlinear thermal stress analysis of surface mount solder joints. Proc. 40th IEEE ECTC 2, 959–972.

Pao, Y.-H., 1992. A fracture mechanics approach to thermal fatigue life prediction of solder joints. IEEE Transactions on Components, Hybrids, and Manufacturing Technology 15 (4), 559–570.

Predel, B., 1997. Phase Equilibria, Crystallographic and Thermodynamic Data of Binary Alloys, vol. 5. Springer, Berlin, Germany (subvolume I Ni–Np...Pt–Zr).

Raghavan, V., Cohen, M., 1975. Solid-state phase transformations. In: Hannay, N.B. (Ed.), Treatise on Solid State Chemistry, Changes of State, vol. 5. Plenum Press, New York, London, pp. 67–127.

Raynor, G.V. 1965. Phase diagrams and their determination. In: Cahn, R.W. (Ed.), Physical Metallurgy. North-Holland, Amsterdam, pp. 291–363.

Rothman, S.J. 1984. The measurement of tracer diffusion coefficients in solids. In: Murch, J.E., Nowick, A.S. (Eds.), Diffusion in Crystalline Solids. Academic Press, Orlando.

Seyyedi, J., Arsenault, B., Keller, J.P., 1991. Stress-rupture and creep behaviour of 63Sn–37Pb production soldered connections. Soldering and Surface Mount Technology 7, 49–55.

Sundquist, B.E., 1964. A direct determination of the anisotropy of the surface free energy of solid gold, silver, copper, nickel, and alpha and gamma iron. Acta Metallurgica 12, 67–86.

Suquet, P., 1990. Une méthode simplifiée pour le calcul de propriétés élastiques de matériaux hétérogènes à structure périodique. C. R. Acad. Sci. Paris 311 (2), 769–774.

Takeuchi, A., Koyama, T., Kazakai, T., Miyazaki, T., 1990. Computer simulation of phase decomposition in th eregular solid solution based upon the non-linear diffusion equation. J. Japan Inst. Metals 54 (11), 1177–1182.

Tsakalakos, T., 1985. On certain phase transition related problems in metallurgy. pp. 149–184.

Wang, Y., Khachaturyan, A.G., 1995. Shape instability during precipitate growth in coherent solids. Acta Metall. Mater 43 (5), 1837–1857.

Wang, Y., Khachaturyan, A.G., 1997. Three-dimensional field model and computer modeling of martensitic transformations. Acta Metall. Mater 45 (2), 759–773.

Wang, Y., Chen, L.-Q., Khachaturyan, A.G., 1991. Strain-induced modulated structures in two-phase cubic alloys. Scripta Metallurgica et Materialia 25, 1969–1974.

Wang, Y., Chen, L.-Q., Khachaturyan, A.G., 1993a. Kinetics of strain-induced morphological transformation in cubic alloys with a miscibility gap. Acta Metall. Mater 41 (1), 279–296.

Wang, Y., Wang, H., Chen, L.-Q., Khachaturyan, A.G., 1993b. Shape evolution of a coherent tetragonal precipitate in partially stabilized cubic $ZrO_2$: a computer simulation. The Journal of the American Ceramic Society 76 (12), 2029–3033.

Wang, Y., Wang, H., Chen, L.-Q., Khachaturyan, A.G., 1994. Computer simulation of microstructure evolution in coherent solids. In: Johnson, W.C., Howe, J.M., Laughlin, D.E., Soffa, W.A. (Eds.), Solid → Solid Phase Transformations. The Minerals, Metals and Materials Society, Warrendale, Pennsylvania 15086, pp. 245–265.

Winter, M., 1998. WebElements™. University of Sheffield, http://www.shef.ac.uk/chemistry/web-elements/.